PROJECTING FUTURE SEA LEVEL

WHITE PAPER

A Report From:
California Climate Change Center

Prepared By:
Dan Cayan, Peter Bromirski, Katharine Hayhoe, Mary Tyree, Mike Dettinger, and Reinhard Flick

Arnold Schwarzenegger, *Governor*

March 2006
CEC-500-2005-202-SF

Acknowledgements

We acknowledge the international modeling groups for providing their data for analysis, the Program for Climate Model Diagnosis and Intercomparison (PCMDI) for collecting and archiving the model data, the JSC/CLIVAR Working Group on Coupled Modeling (WGCM) and their Coupled Model Intercomparison Project (CMIP) and Climate Simulation Panel for organizing the model data analysis activity, and the IPCC WG1 TSU for technical support. The IPCC Data Archive at Lawrence Livermore National Laboratory is supported by the Office of Science, U.S. Department of Energy. In particular, we thank the NOAA Geophysical Fluids Dynamics Laboratory global modeling group, and the NCAR/DOE Parallel Climate Modeling group for very responsive model output and consultation. We thank Douglas Inman and David Jay for reviewing the manuscript.

Preface

The Public Interest Energy Research (PIER) Program supports public interest energy research and development that will help improve the quality of life in California by bringing environmentally safe, affordable, and reliable energy services and products to the marketplace.

The PIER Program, managed by the California Energy Commission (Energy Commission), annually awards up to $62 million to conduct the most promising public interest energy research by partnering with Research, Development, and Demonstration (RD&D) organizations, including individuals, businesses, utilities, and public or private research institutions.

PIER funding efforts are focused on the following RD&D program areas:

- Buildings End-Use Energy Efficiency
- Energy-Related Environmental Research
- Energy Systems Integration
- Environmentally Preferred Advanced Generation
- Industrial/Agricultural/Water End-Use Energy Efficiency
- Renewable Energy Technologies

The California Climate Change Center (CCCC) is sponsored by the PIER program and coordinated by its Energy-Related Environmental Research area. The Center is managed by the California Energy Commission, Scripps Institution of Oceanography at the University of California at San Diego, and the University of California at Berkeley. The Scripps Institution of Oceanography conducts and administers research on climate change detection, analysis, and modeling; and the University of California at Berkeley conducts and administers research on economic analyses and policy issues. The Center also supports the Global Climate Change Grant Program, which offers competitive solicitations for climate research.

The California Climate Change Center Report Series details ongoing Center-sponsored research. As interim project results, these reports receive minimal editing, and the information contained in these reports may change; authors should be contacted for the most recent project results. By providing ready access to this timely research, the Center seeks to inform the public and expand dissemination of climate change information; thereby leveraging collaborative efforts and increasing the benefits of this research to California's citizens, environment, and economy.

For more information on the PIER Program, please visit the Energy Commission's website www.energy.ca.gov/pier/ or contact the Energy Commission at (916) 654-5164.

Table of Contents

List of Figures

List of Tables

Abstract

California's coastal observations and global model projections indicate that California's open coast and estuaries will experience increasing sea levels over the next century. Sea level rise has affected much of the coast of California, including the Southern California coast, the Central California open coast, and the San Francisco Bay and upper estuary. These trends, quantified from a small set of California tide gages, have ranged from 10–20 centimeters (cm) (3.9–7.9 inches) per century, quite similar to that estimated for global mean sea level. So far, there is little evidence that the rate of rise has accelerated, and the rate of rise at California tide gages has actually flattened since 1980, but projections suggest substantial sea level rise may occur over the next century.

Climate change simulations project a substantial rate of global sea level rise over the next century due to thermal expansion as the oceans warm and runoff from melting land-based snow and ice accelerates. Sea level rise projected from the models increases with the amount of warming. Relative to sea levels in 2000, by the 2070–2099 period, sea level rise projections range from 11–54 cm (4.3–21 in) for simulations following the lower (B1) greenhouse gas (GHG) emissions scenario, from 14–61 cm (5.5–24 in) for the middle-upper (A2) emission scenario, and from 17–72 cm (6.7–28 in) for the highest (A1fi) scenario. In addition to relatively steady secular trends, sea levels along the California coast undergo shorter period variability above or below predicted tide levels and changes associated with long-term trends. These variations are caused by weather events and by seasonal to decadal climate fluctuations over the Pacific Ocean that in turn affect the Pacific coast. Highest coastal sea levels have occurred when winter storms and Pacific climate disturbances, such as El Niño, have coincided with high astronomical tides.

This study considers a range of projected future global sea level rises in examining possible impacts at California coastal and estuarine stations. Two climate models and three scenarios considered in this scenarios study provide a set of possible future weather and short-period climate fluctuations, and a range of potential long-term sea level rise values. A range of mean sea level rise was considered in combination with weather and El Niño fluctuations extracted from two global climate models and two GHG emissions scenarios. The mean sea level rise values, determined from a survey of several climate models, range from approximately 10–80 cm (3.9–31 in) between 2000 and 2100. The middle to higher end of this range would substantially exceed the historical rate of sea level rise of 15–20 cm (5.9–7.9 in)per century observed at San Francisco and San Diego during the last 100 years. Gradual sea level rise progressively worsens the impacts of high tides and the surge and waves associated with storms. The potential for impacts of future sea level rise was assessed from the occurrence of hourly sea level extremes. The occurrence of extreme events follows a sharply escalating pattern as the magnitude of future sea level rise increases. The confluence of Low barometric pressures from storms and the presence large waves at the same time substantially increases the likelihood of high, damaging sea levels along the California coast. Similarly, astronomical tides and disturbances in sea level that are caused by weather and climate fluctuations are

transmitted into the San Francisco Bay and Delta, and on into the lower reaches of the Sacramento River. In addition to elevating Bay and Delta sea levels directly through inverse barometer and wind effects, storms may generate heavy precipitation and high fresh water runoff and cause floods in the Sacramento/San Joaquin Delta, increasing the potential for inundation of levees and other structures. There may also be increased risk of levee failure due to the hydraulics and geometry of these structures. Rising sea levels from climate change will increase the frequency and duration of extreme high water levels, causing historical coastal and San Francisco Bay/Delta structure design criteria to be exceeded.

1.0 Pre-instrumental Sea Level

Pre-instrumental historical changes in sea level are based on geological data, summarized here from the IPCC 2001 report (Church et al. 2001). Since the last glacial maximum, approximately 18,000 years ago, global sea level has risen approximately 120 meters (m) (394 feet, ft) (Fairbanks 1989). Global average sea level appears to have risen at an average rate of about 5 centimeters (cm) (2 inches, in) per century over the last 6,000 years, and at an average rate of 1–2 cm (0.4–0.8 in) per century over the last 3,000 years (Church et al. 2001).

Based on tide gauge data, the rate of global average sea level rise (SLR) during the twentieth century is in the range 10–20 cm (3.9–7.9 in) per century. From the few very long tide gauge records, the average rate of SLR has been larger during the twentieth century than the nineteenth century. However, no significant acceleration in the rate of SLR during the twentieth century has been detected (Church et al. 2001). While there is decadal variability in extreme sea levels, there is no evidence of widespread increases in extremes other than that associated with a change in the mean.

Global average sea level is affected primarily by two factors. First, thermal expansion (TE) due to higher water temperatures leads to an increase in ocean volume at constant mass. Observational estimates of the TE component of SLR average less than about ~10 cm (~3.9 in) per century over recent decades. These are similar to values of 7.4–11 cm (2.9–4.3 in) per century obtained from medium-resolution coupled atmosphere-ocean climate models over a comparable period, although lower-resolution models tend to over-estimate the rate of TE by about a factor of two (Figure 1). Averaged over the twentieth century, climate model simulations result in rates of thermal expansion of 3–7 cm (1.2–2.8 in) per century.

Second, the mass of the ocean, and thus sea level, changes as water is exchanged with glaciers and land grounded ice caps such as Antarctica and Greenland. Observational and modeling studies of glaciers and ice caps indicate a contribution to sea level rise of 2 to 4 cm per century averaged over the twentieth century. The sum of these components indicates a rate of total SLR (corresponding to a change in ocean volume) from 1910 to 1990 ranging from –8 to 22 cm (-3–8.7 in) per century, with a central value of 7 cm (2.8 in) per century. The upper bound is close to the observational upper bound (20 cm or 7.9 in per century), but the central value is less than the observational lower bound (10 cm or 3.9 in per century), i.e., the sum of model components is biased low compared to observations or estimates from observations. The estimated rate of SLR from anthropogenic climate change from 1910 to 1990 (from modeling studies of thermal expansion, glaciers, and ice sheets) ranges from 3 to 8 cm (1.2–3.1 in) per century. It is very likely that twentieth century warming has contributed significantly to the observed SLR, through both the thermal expansion of sea water and as well as widespread loss of land ice.

Land movements, both isostatic and tectonic, will continue through the twenty-first century at rates which are probably unaffected by climate change. However, if the rate of sea level rise accelerates through the coming century, it can be expected that by 2100 some regions currently experiencing relative sea level fall, for example due to isostatic

rebound of the Earth's crust following deglaciation, will instead experience rising relative sea levels.

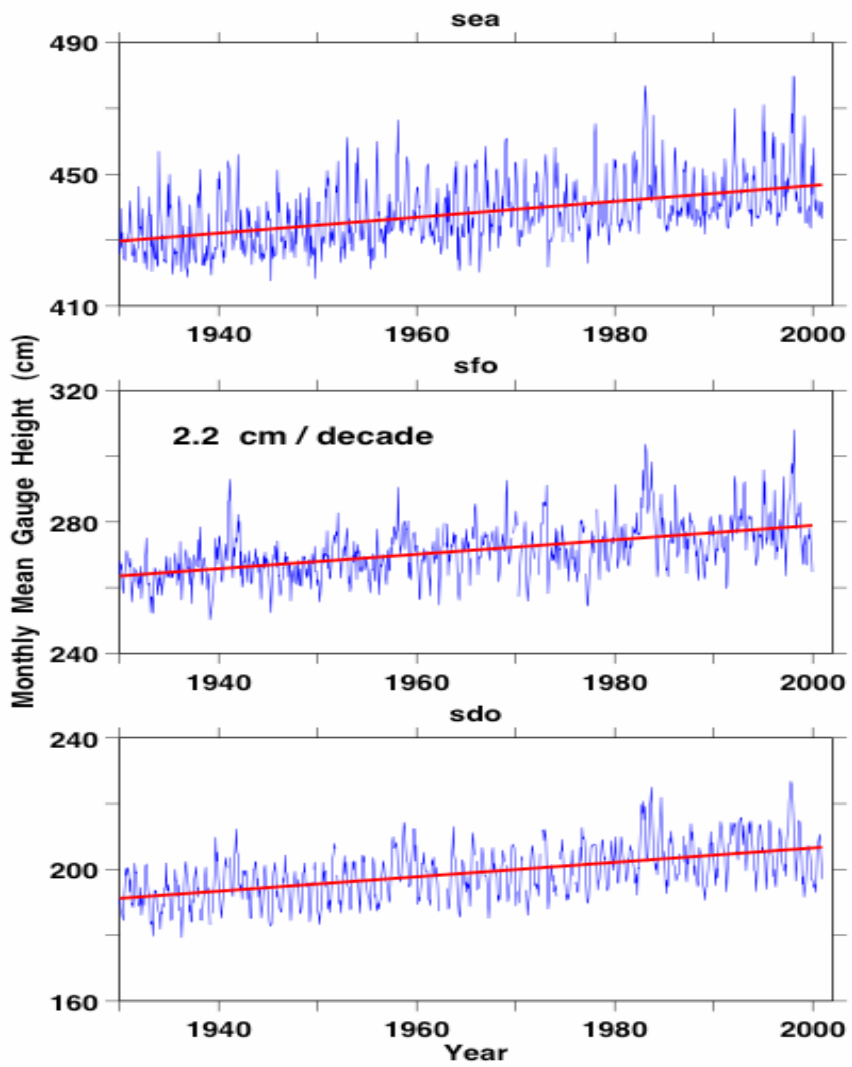

Figure 1. Observed sea level (cm) from Seattle, San Francisco, and San Diego tide gages.

2.0 Recent Sea Level Change

Sea level observed at the longest tide gauge records along the West Coast shows consistent upward trends of about 20 cm (8 in) per century, as shown in Figure 1. These rates of SLR are consistent with those estimated for global sea level during the last several decades (Barnett 1984; Chambers et al. 2002; Church et al. 2004) and are at the upper bound of the IPCC (Church et al. 2001) range.

Our study to project future sea level variability, particularly extremes, is based upon observed sea level at a small set of relatively long-lived tide gauges along the California coast (Figure 1), at Crescent City, San Francisco, and La Jolla. The distributions of observed sea levels for the period of available record at these stations, relative to mean sea level over the 1960–1978 tidal epoch, are shown in Figure 2. On one hand, at Crescent City, the occurrence of sea level extremes has decreased slightly over the available record, evidently in response to tectonic activity causing coastal uplift along portions of the northern California coast. However, at coastal locations that are more tectonically stable, the occurrence of extremes has increased markedly. This includes San Francisco (by twentyfold since 1915) and at La Jolla (by thirtyfold since 1933). It is expected that these exceedances may become even more common, since the middle and higher end of projected rates of SLR over 2000–2100 exceed the rate of SLR observed during the last century. Sea level histories from 1930–2000 at Seattle, San Francisco, and San Diego are shown in Figure 1.

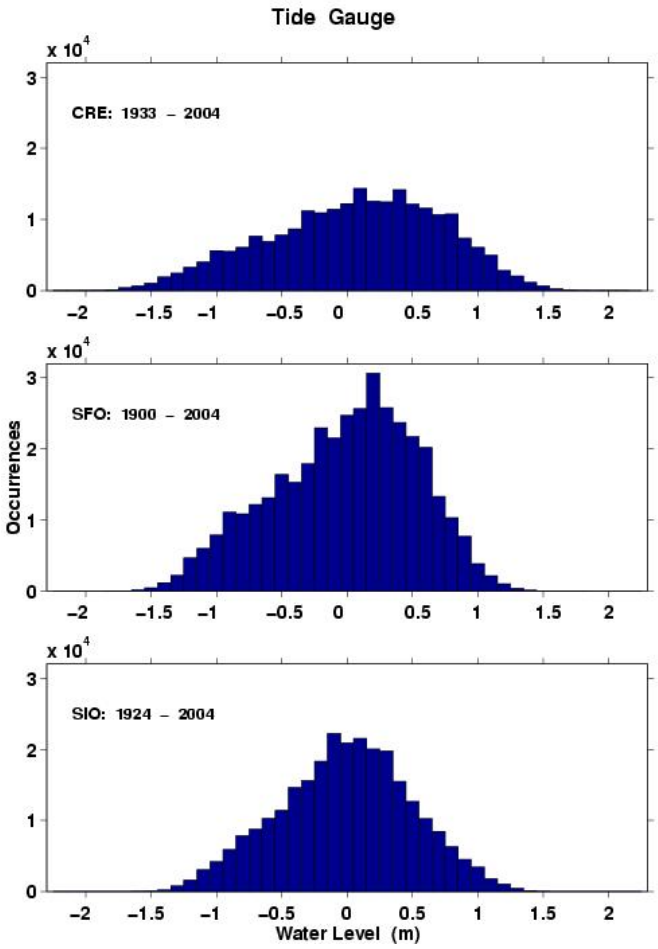

Figure 2. Distributions of sea level height (m) relative to 1960–1978 mean sea level at Crescent City, San Francisco, and La Jolla.

3.0 Projected Global Sea Level Rise

As discussed in Section 1, global sea level is rising due to two factors, both of which are affected by temperature increases: thermal expansion of sea water and additional water from melting continental ice sheets and glaciers. Over the next few hundred years, as global climate warms, it is broadly anticipated (Church et al. 2001) that global sea level will rise by several feet as the earth's stock of ground-based ice, such as in Greenland and Antarctica, melts.

Updated estimates of the projected range in SLR over the next century due to thermal expansion have recently become available for the IPCC Special Report on Emissions Scenarios (SRES) A2 and B1 scenarios. However, the component of SLR due to ice melt (due to melt from Antarctica, Greenland, and glaciers) has not yet been calculated for these latest Atmosphere-Ocean General Circulation Model (AOGCM) simulations. Because ice melt is an important component of global SLR (currently accounting for ~37% to 60% of observed changes, based on observations and modeling over the last century), it is essential to have some estimate of this value in order to evaluate the overall effect of SLR on the California coast.

Here, we use the relationship between projected global mean temperature change, SLR due to thermal expansion (TE), and SLR due to ice melt (IM) based on the relationships provided by the MAGICC model (Hulme et al. 1995). The starting point uses current-day estimates of the relative contribution of thermal expansion versus ice melt compared to observed SLR over the past century (Figure 3). These percentages were then taken as the base values for 1990, and the relative change of the IM-to-TE components over time was derived from MAGICC simulations from 1990 to 2100, as shown in Figure 3. Estimates were made for IM, and also for the range in total SLR projections for the A2 and B1 greenhouse gas emission scenarios (Nakicenovik et al. 2000).

Sea level rise projections for the A1fi scenario are not yet available from the new AR4 simulations. Here, MAGICC-based A1fi projections for thermal expansion were scaled down based on the relative reduction in A2 projections from the new AR4 simulations as compared with previous MAGICC-based A2 projections. The ice melt component was then calculated using the same approach as described above.

As shown in Figure 4 and Table 1, by mid-century (2035–2064) projected global SLR ranges from ~6-32 cm (2.4-12.6 in) relative to 1990, with no discernable inter-scenario differences. By end-of-century (2070–2100), however, total (thermal expansion + ice melt) SLR projections range from 10–54 cm (3.9-21.3 in) under B1 to 14–61 cm (5.5-24 in) under A2, and 17–72 cm (6.7-28.3 in) under A1fi, as shown in Table 2.

There is considerable uncertainty in estimates of recent global mean sea level (MSL) rise, and also considerable variation in estimates between different regions. The IPCC (Church et al. 2001) report gives the range of sea level rise from 10–20 cm (3.9-7.9 in)per century, of which the eustatic component (added water from melting glaciers and continental ice sheets) is about 3–6 cm (1.2-2.4 in) per century. Munk (2002) suggests possible explanations for discrepancies between the rate of estimated MSL rise and the

sum of the steric (thermal expansion) and eustatic components, estimated at 6 cm (2.4 in) per century steric and 3 cm (1.2 in) per century (Douglas and Peltier 2002). As the total of estimated steric and eustatic estimates are at the lower end of the IPCC (Church et al. 2001) range, the commonly accepted estimate of 20 cm (7.9 in) per century may be too high as a consequence of the global distribution of tide gauges used for estimation (Cabanes et al. 2001), with some regions experiencing MSL rise rates twice that of others. In that light, it is important to consider strongly the local estimates of sea level rise in regional studies such as along the California coast.

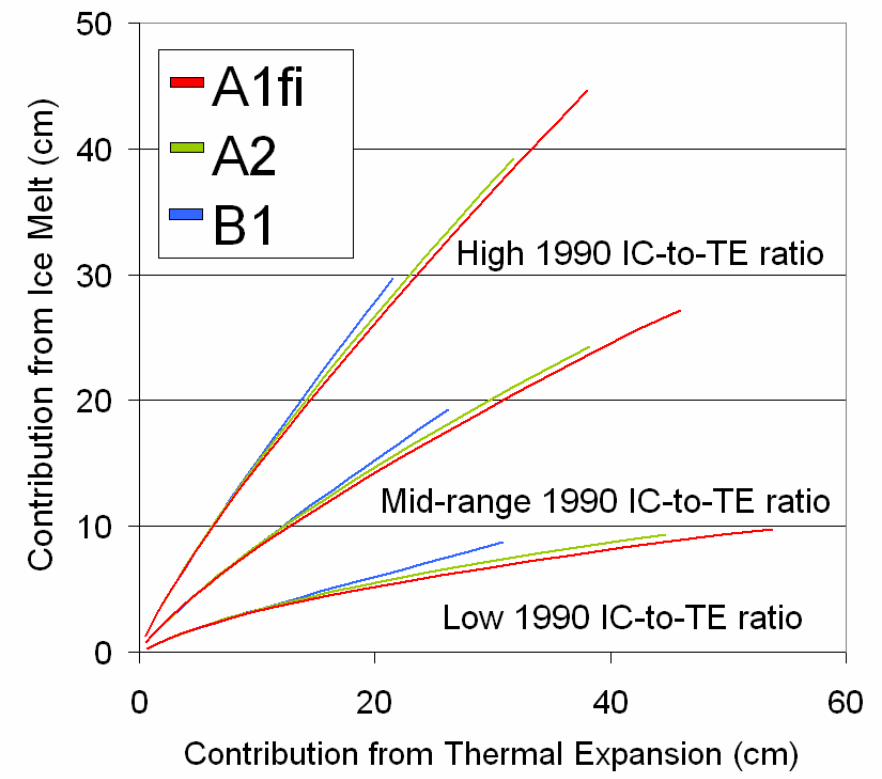

Figure 3. MAGICC-simulated relationship between the relative contributions of ice melt and thermal expansion to global sea level rise estimates over the next century, corresponding to the range of historical ratios derived from observational and modeling studies

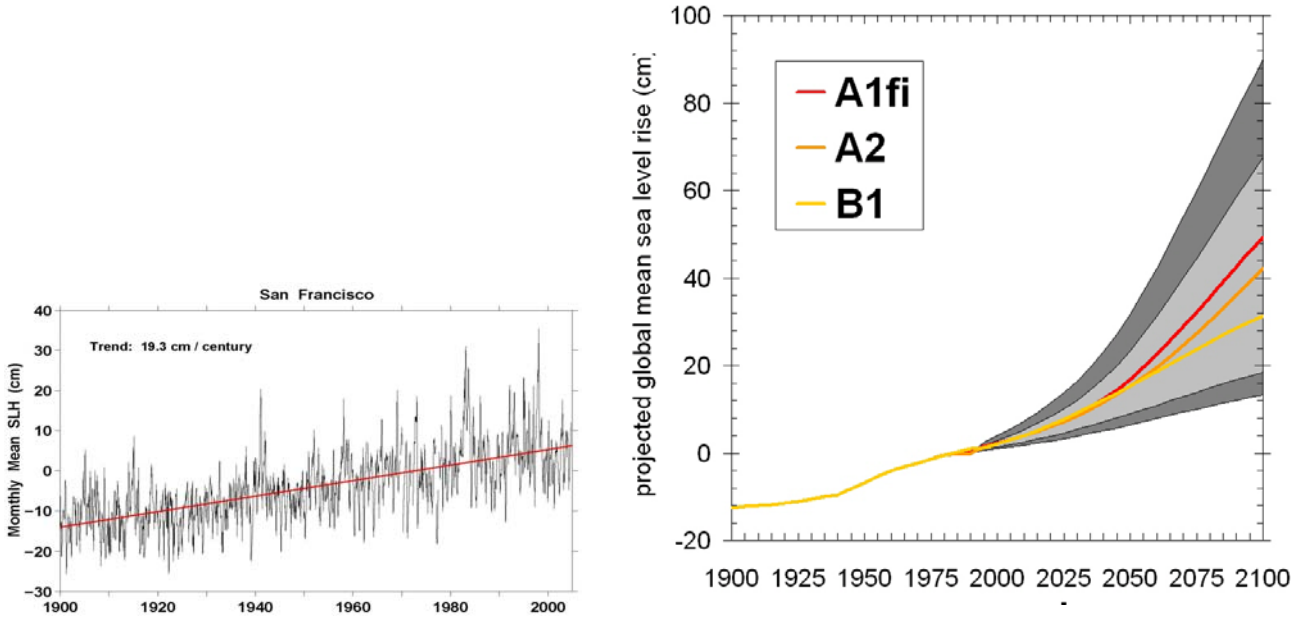

Figure 4. Projected sea level rise from climate model estimates for three GHG emissions scenarios: A1fi (high emissions), A2 (medium-high emissions), and B1 (low emissions). San Francisco-observed sea level, with trend of 19.3 cm/century, is shown for comparison.

3.1. Tides on the California Coast

Tides are regular changes of ocean water levels caused by the gravitational forces of the moon and sun. Because of the orbital mechanics involved and the rotation of the earth, the dominant tidal oscillations show up at 1 and 2 cycles per lunar day (24 hours, 50 minutes). The tide is the only component of sea level change that is accurately predictable and has the largest magnitude, with open coast elevation changes in California of up to about 10 ft (3 m). Most of the "spread" in the distribution of elevations about mean sea level in Figure 2 are caused by tides.

Many other fluctuations contribute to local sea level changes. Additional factors include storm surges, large scale changes in water temperature and wind forcing, climate-related fluctuations, and long-term rise in relative sea level (Flick and Cayan 1984).

Table 1. Observed high sea level occurrences from three California coast tide gauge records. 99.9th and 99.99th percentile thresholds from 1933–2004 hourly observations.

Crescent City

Thresholds: 99.9th percentile = 1.529m, 99.99th percentile = 1.744m

Period (yr)	# > 99.9th	# > 99.99th	Max (m)	# Obs
1915–1933				
1933–1951	132	8	1.78819	117574
1951–1969	139	17	1.94019	149020
1969–1987	174	23	2.14119	145668
1987–2004	120	8	1.84219	145227

San Francisco

Thresholds: 99.9th percentile = 1.228m, 99.99th percentile = 1.410m

Period (yr)	# > 99,9th	# > 99.99th	Max (m)	# Obs
1915–1933	15	1	1.43427	157798
1933–1951	45	5	1.44627	157776
1951–1969	100	7	1.45627	157137
1969–1987	264	36	1.80027	155396
1987–2004	349	29	1.68027	149016

La Jolla (Scripps Pier)

Thresholds: 99.9th percentile = 1.290m, 99.99th percentile = 1.412m

Period (yr)	# > 99.9th	# > 99.99th	Max (m)	# Obs
1915–1933				
1933–1951	11	0	1.31815	148375
1951–1969	79	3	1.47315	144392
1969–1987	191	29	1.52515	145562
1987–2004	327	24	1.54615	148320

On the California coast, tides are mixed, periodically having nearly equal semi-daily and daily components. Zetler and Flick (1985a,b; Flick 1986) have described a number of interesting consequences of this mixed tide regime. California's tide regime is distinctly different from the semi-diurnal conditions that dominate the east coast of the United States. The most important tidal fluctuations on the California coast occur once and twice daily, twice monthly, twice yearly, and every 4.4 years.

The two high tides and two low tides that occur each day are, respectively, unequal in amplitude, as seen for example in Figure 5. The lower-low tide of the day generally follows the higher-high after about 7 or 8 hours. The rise from lower-low to the next higher-high (through lower-high and higher-low) takes the rest of the tidal day, or about 17 hours.

The monthly tidal changes are dominated by the spring-neap cycle, with two periods of relatively high tides (springs) around full and new moon, and two periods of lower ranges (neaps) around the times of half-moon. One spring tide range per month is usually higher than the other on this coast, a consequence of the moon's distance and declination.

The highest monthly tides in the winter and summer months are higher than those in the spring and fall as a result of lunar and solar declination effects. The respective differences can range up to about 1.6 ft (0.5 m). Furthermore, the extreme monthly higher-high tides in the winter tend to occur in the morning, sometimes quite early (Flick 2000). This is a disadvantage from a coastal flooding perspective, because preparations for storm waves must often be made at night, in anticipation of the higher-high tide the next morning.

Longer period variations also occur in the tides. On the California coast, there is a distinct 4.4-year cycle that results in higher peak monthly tides of about 0.5 ft (0.15 m), compared with years in between. This cycle peaked in 1982–1983, 1986–1987, 1990–1991, 1995–1996, and 1999–2000, etc. Recently, a secular trend has been documented in the tide range along much of the California coast (Flick et al. 2003). This means that high tide levels are rising faster than mean sea level for reasons that are not yet understood. For example, at San Francisco, the rate of increase in mean higher high water (MHHW) was 20% greater than the rate of sea level rise over the past century.

Storm surge is that portion of the local, instantaneous sea level elevation that exceeds the predicted tide and which is attributable to the effects of low barometric pressure and high wind associated with storms. Sometimes the super-elevation of sea level due to waves and wave-induced surges is included in design calculations of storm surge, particularly for structures on beaches. Storm surge along the California coast, excluding the effect of waves, rarely exceeds 1 ft (0.3 m) in amplitude (Flick and Badan-Dangon 1989; Flick 1998). However, wave-induced surge on a beach can be of the order of the significant breaker height, which can reach 5 or 6 ft (1.5 or 1.8 m) during large wave events.

(a)

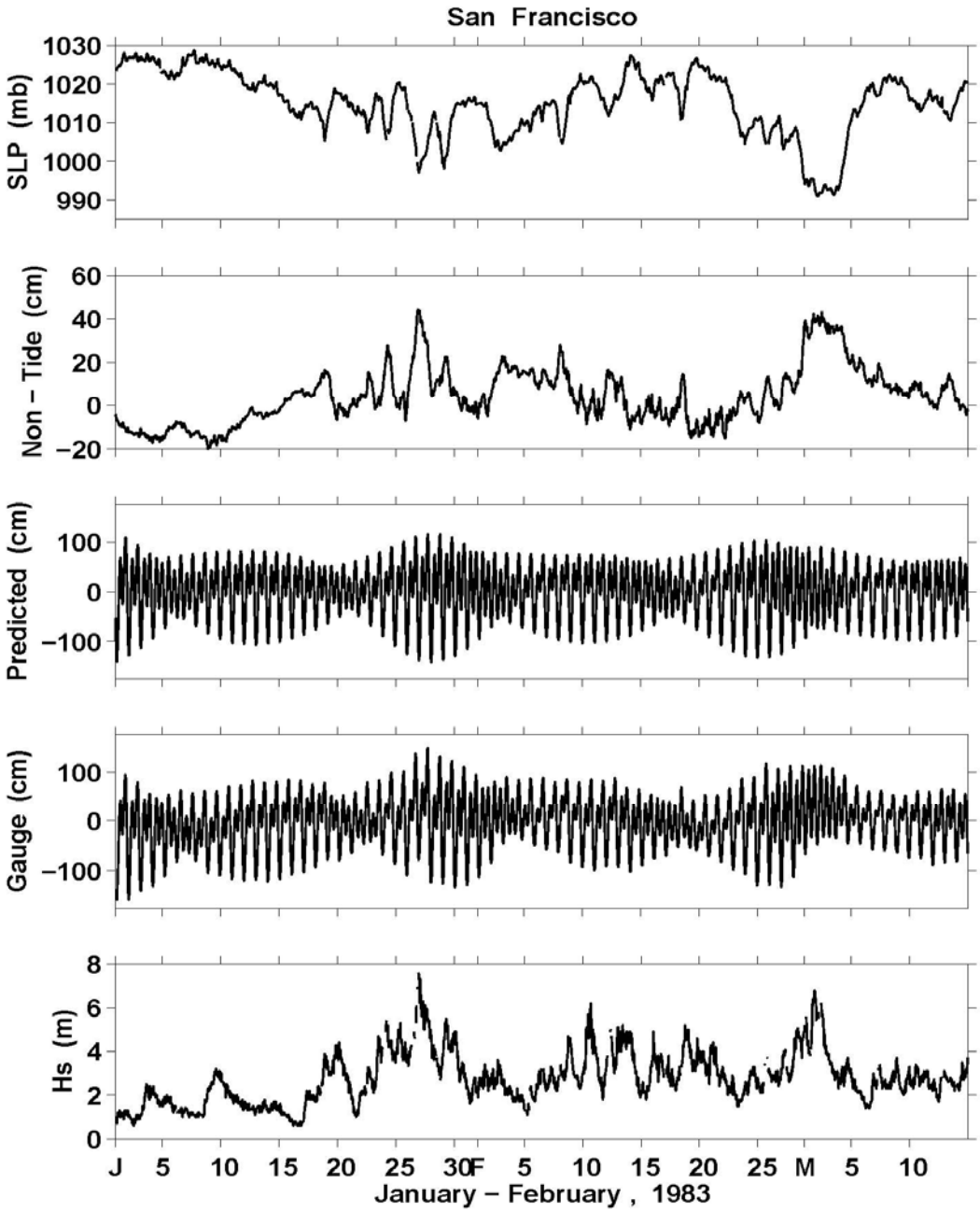

Figure 5. San Francisco SLP, non-tide sea level anomaly, predicted tides, total sea level, and significant wave height (Hs) during winter of (a) 1983, and (b) 1998. Sea level is from the San Francisco tide gage at The Presidio (Bromirski et al. 2003). SLP is from NOAA Buoy 46026, with data from Buoy 46014 substituted in during March 1983, when Buoy 46026 was out of operation.

b)

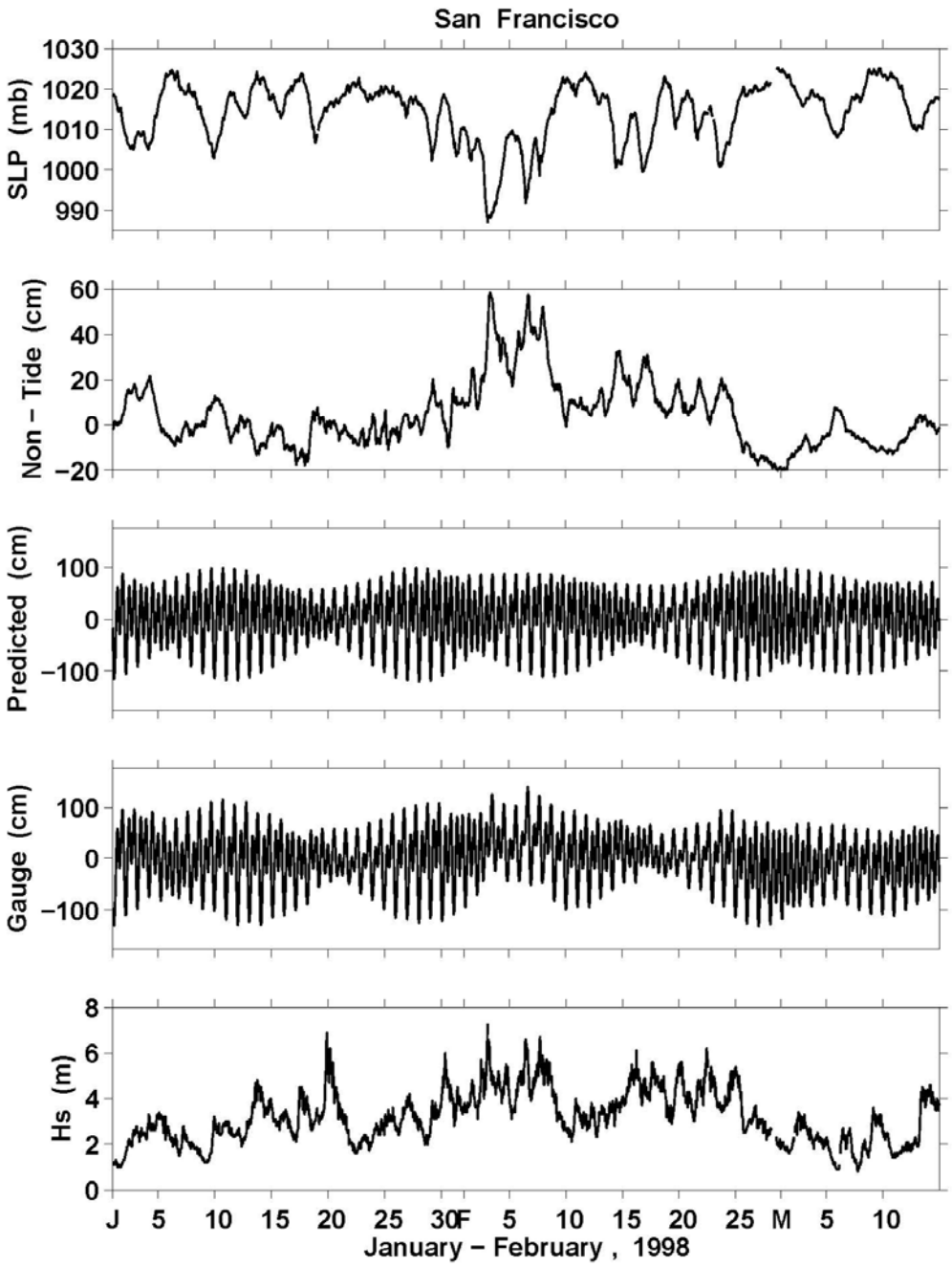

Figure 5. (continued).

4.0 Atmospheric Teleconnection Patterns and Winter Storms

Several factors come into play in producing high coastal sea level inundation. These events usually occur during winter storms under the joint occurrence of high sea levels during high tides and high waves. Seasonally, higher sea levels naturally occur during autumn and winter due to seasonal wind patterns, and upwelling along the California coast. Then, high tides that occur at new or full moons can raise base sea level by more than one meter, enhancing storm surge heights if they occur at that time. Next, the low pressure that accompanies winter storms also allows the ocean surface to rise, raising sea level, since a one millibar (mb) decrease in pressure is equivalent to a one cm rise in sea level. An intense winter storm could raise sea level by up to 25 centimeter (10 inches) along the California coast (Ryan 2000). Finally, all these factors can contribute to enhance the wind-forced storm surges and high waves that are actually generated by the storm. The additive effects of storms, tides, waves, and El Niño/Southern Oscillation (ENSO) events on sea level were quite remarkable during the massive ENSO winters of 1982–1983 and 1997–1998, shown in Figures 5a and 5b.

Winter storms and flooding in southern California in particular are strongly linked to warm sea surface temperatures and ENSO events (Diaz et al. 2001; Cayan et al. 1999; Dettinger et al. 2000; Dettinger et al. 2001; Andrews 2004). Paleo-records confirm that this relationship extends back several millennia (Ely et al. 1997; Moy et al. 2002; Cobb et al. 2004; Tudhope and Collins 2003) and probably over the last 130,000 years (Tudhope et al. 2001; Cane 2005), and indicate that ENSO has varied substantially within pre-industrial epochs from mechanisms associated with internal variability. Future climate simulations that contain the effects of greenhouse gas forcing indicate that ENSO will remain active during climate warming, but it is unsettled whether the frequency of ENSO might change or whether the strength and amplitude of ENSO variations will strengthen or weaken (Cubash and Meehl 2001). During El Niño events, the California coast has been affected by high sea levels and high waves (Westerling 2001; Bromirski et al. 2003; Bromirski et al. 2005), heavy rainfall events and large floods (Cayan et al. 1999; Masutani and Leetmaa 1999; Andrews et al. 2004). El Niño enhances effects of winter storms along the California coast through first weakening trade winds, creating a warm sea surface temperature anomaly along the California coast that temporarily raises local and global sea level due to thermal expansion and dynamical effects (see Figure 5a,b and Figure 6a), above that which is already occurring due to climate change (NOAA 2004; Nerem et al. 1999; Cayan et al. 1997). Next, changes in atmospheric pressure and wind patterns associated with El Niño events elevate both the frequency and intensity of winter storms. In addition, the effect of low-pressure systems on sea level mentioned above is magnified by the Earth's Coriolis effect as ENSO-driven winds blow in primarily from the south during fall and winter (Ryan 2000). Finally, Kelvin waves are generated in the tropical western Pacific during El Niño events. These waves move northward up the California coast, bring an influx of warm water and raise sea level by 6–10 inches (15–25 cm) as they pass (Enfield and Allen 1980).

The most severe coastal impacts are likely to occur under a combination of storm-driven surges and extreme waves that last for several days, very intense low-pressure autumn or winter storms, and high tides (Bromirski et al. 2003). The best near-term example of

the influence of the El Niño on southern California was demonstrated during the event of 1997–1998 that created a series of severe winter storms with damages in the hundreds of millions of dollars (Ryan 2000). During one of the storms in February 1998, all of the factors listed above coincided to raise sea level by up to five ft (1.5 m) above normal in the San Francisco Bay.

Although all strong El Niño events tend to produce more frequent winter storms, non-El Niño years can also produce elevated sea heights, wave energy, and anomalously high or low precipitation due to other atmospheric circulation patterns (Figure 6b), including the Pacific Decadal Oscillation (PDO) (Mantua et al. 1997), the North Pacific Cyclone index (NP) (Trenberth and Hurrell 1994), and the Pacific North American Pattern (PNA) (Bromirski et al. 2003, 2005; Cayan 1996; Robertson and Ghil 1999).

This portion of the paper assesses projected changes in three of the major teleconnection patterns (ENSO, PNA, and NP cyclone index) under conditions of future change as simulated by the GFDL and PCM models for the SRES A2 (mid-high) and B1 (lower) scenarios (Figures 7a and 7b) to demonstrate how these are likely to influence coastal California over the coming century.

The ENSO 3.4 index was used to represent variations in the El Niño-Southern Oscillation. There are several indices available to calculate ENSO, but this index was selected as being relatively straightforward to calculate from model simulations. It is also potentially more sensitive to La Niña events (Hanley et al. 2003), of which some models suggest that may occur less frequently during the coming century (Figure 7a).

The ENSO 3.4 index is calculated from sea surface temperatures over the region from 5°S–5°N and from 170°W–120°W. The region displays large variability on El Niño time scales, and is relatively close to the area where changes in local sea-surface temperature are important for shifting the large region of rainfall typically located in the far western Pacific.

The Pacific North American Pattern was calculated using Rotated Principal Component Analysis (RPCA) based on geopotential height fields as described in Barnston and Livezey (1987). The RPCA technique was applied to monthly mean standardized 500 mb height anomalies output from the PCM and GFDL models for the Northern Hemisphere above 20°N. Researchers first determined the unrotated empirical orthogonal functions from the monthly height anomaly fields in the three-month period centered on that month, then performed a varimax rotation on the two leading un-rotated modes and standardized by monthly means to produce the time series for PNA (the second principal component). Finally, the NP Cyclone index is calculated from the area-weighted sea level pressure over the region 30°N–65°N, 160°E–140°W.

The first step is to compare trends based on historical observations with those simulated by the AOGCMs for the same time period, then to assess the projected future trends over the coming century. Table 2 shows the sign of the trend in the negative and positive phase of the index based on observational evidence and model simulations for the historical period, and based on the SRES A2 and B1 scenarios for the future century.

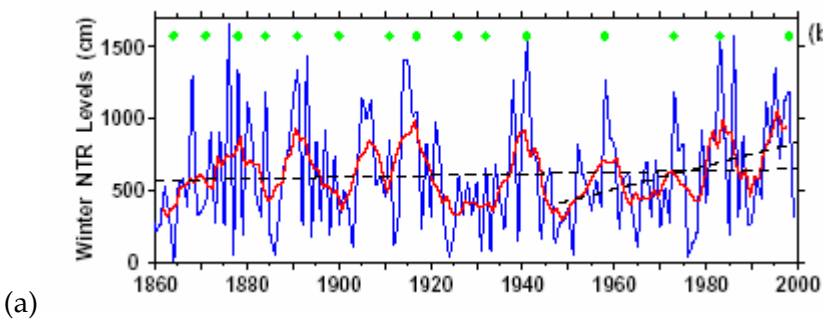

(a)

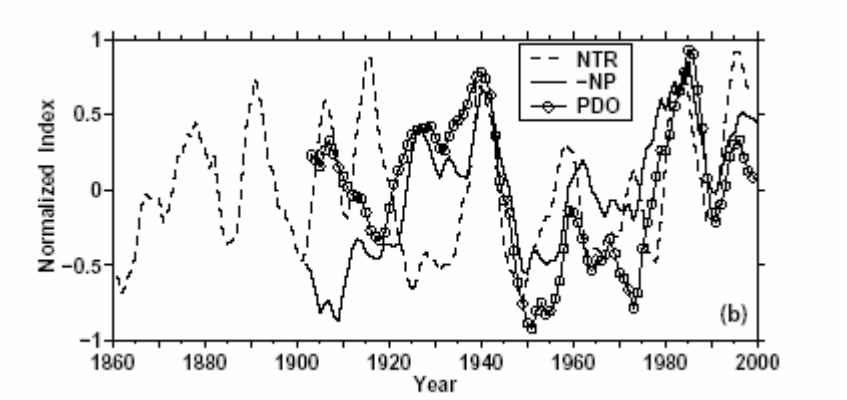

(b)

Figure 6. (a) Cumulative extreme NTR (blue), 5-year running mean (red) and El Niño events (green dots). (b) 5-year normalized running mean of winter extreme NTR (dashed line) with NP (solid) and PDO (circles) indices. From Bromirski et al. (2003).

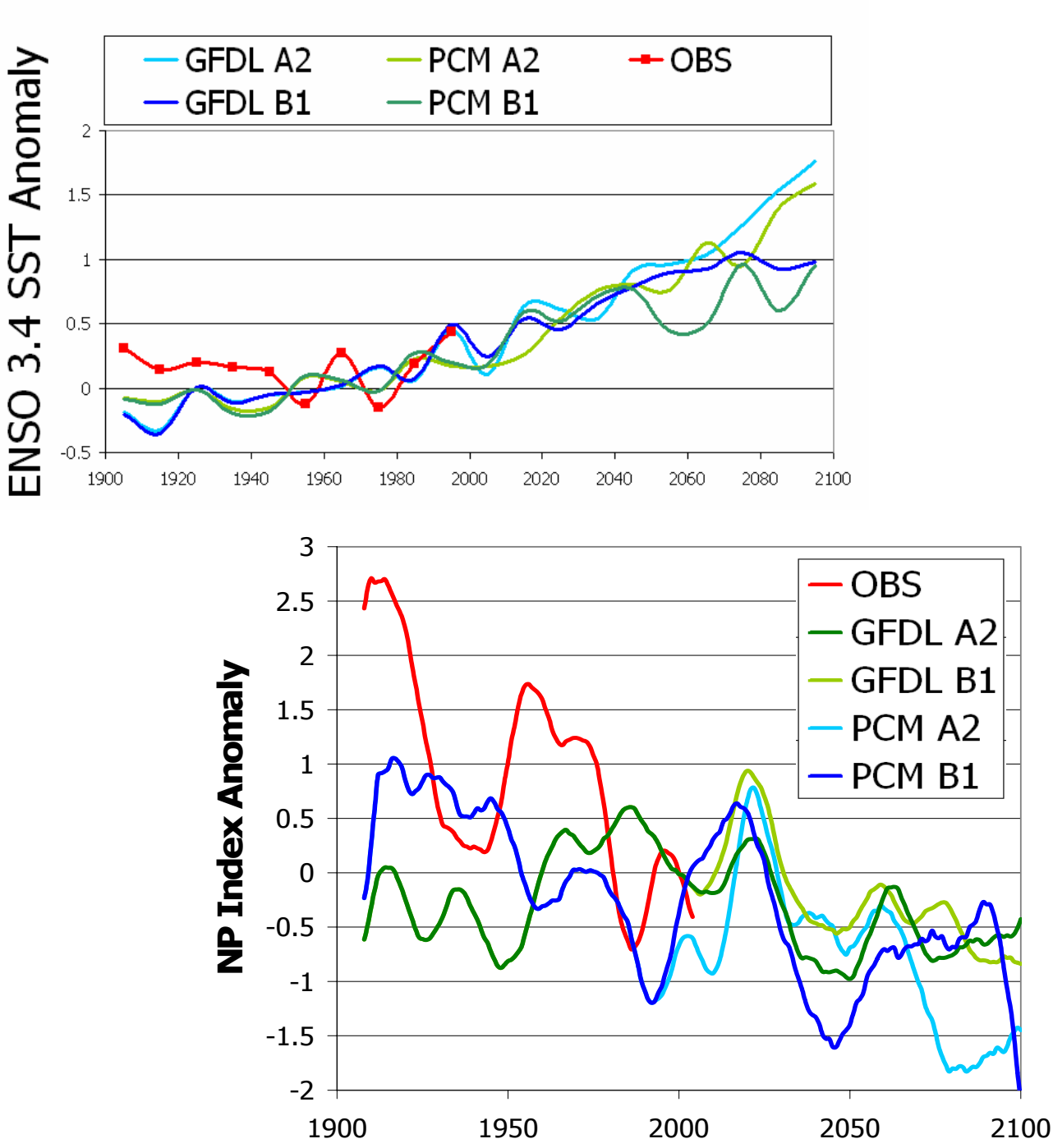

Figure 7. (a) ENSO 3.4 annual SST anomaly relative to 1900–2000 average; these are not detrended series, as were used in some subsequent analyses. Observation-based index shown in red, GFDL in blue, and PCM in green. (b) Anomaly in NP index for November through March relative to 1925–1989 average, 10-year running mean. Observation-based index is shown in red, GFDL simulations in green, and PCM simulations in blue.

Table 2. Comparison of observed with model-simulated trend in positive and negative phases of key atmospheric teleconnection patterns over the historical period. The last two columns are model-simulated changes for the future (2000–2100), while the previous two columns are for the past.

	Observed	PCM historical	GFDL2.1 historical	PCM future	GFDL2.1 future
ENSO					
Positive phase	+	+	+	+	+
Negative phase	-	n/a	n/a	+	+
PNA (1950-2005)					
Positive phase	+	+	+	+	+
Negative phase	+	+	-	-	-
NP (1900-2005)					
Positive phase	-	-	+	-	-
Negative phase	-	-	+	-	-

[1] NP Index Data provided by the Climate Analysis Section, NCAR, Boulder, Colorado. Trenberth and Hurrell (1994).

The observation-based ENSO time series shows no significant linear trend in average value of the index from 1900 to 2000—despite the abrupt and well-documented shift in the mean value of ENSO indices during the mid-1970s (Trenberth and Hoar 1997), resulting in significantly more El Niño events and fewer La Niña events since then. Breaking the time series down into positive and negative components reveals an increasing trend in both the average positive and the average negative value of the ENSO 3.4 index. That is, an increase in intensity of both negative and positive events cancels out, resulting in little or no net change in the average value of the index). The two AOGCMs examined here are able to reproduce the upward trend in the positive phase, but not the trend toward higher negative values. In terms of future trends (2000–2099), both PCM and GFDL indicate significant increases in the average tropical Pacific sea surface temperature, including regions that have been identified as being dynamically active during ENSO. If the trend in the mean sea surface temperature is removed, neither PCM nor GFDL exhibit significant changes in the frequency and/or intensity of the resulting ENSO 3.4 index. However, it is important to note that in-depth studies of the response of simulated ENSO to climate change have found model parameterizations that tend to make ENSO less sensitive to change (Zelle et al. 2005).

For PNA, the historical observation-based time series from 1950–2000 indicate positive changes in the average, positive-phase, and negative-phase values (i.e., stronger positive events; weaker negative events). Both models reproduce the observed increase in the

average positive-phase value over the last five decades (Figure 7b). However, PCM is also able to capture the historical changes in the negative phase and the average value, but GFDL is not. In the future, both models indicate significant increases in the positive phase *and* decreases in the negative phase. This consistency between models suggests that GFDL's failure to reproduce the observed historical trend in the negative phase of the PNA index may arise from over-estimating the influence of climate change during its historical simulations.

For the NP index, observed anomalies are predominantly negative from November to March, and positive from April to October. The observational record indicates a small but insignificant negative trend in positive (summer) anomalies relative to the long-term mean, but a strong downward trend in negative (winter) anomalies. AOGCM results are mixed, with the PCM simulating a comparable downward trend in winter NP anomalies as observed, while GFDL shows an increase over the same time period. In the future, both models show negative (downward) trends in both the positive and negative phases, continuing the observed trend over the last century (Figure 7b).

In summary, observation-based ENSO 3.4, PNA and NP indices all exhibit trends in the historical time series in at least one—if not both—of the primary phases (positive and negative). PCM and GFDL produce reasonable ENSO, PNA, and NP signals and are able to simulate the observed upward trend in positive-phase ENSO and PNA indices, although PCM shows better skill than GFDL at simulating the observed changes in negative PNA and NP. Over the next century, all model and scenario combinations agree on the sign of the trend for each of these indices, with ENSO becoming predominantly positive (due to the increase in sea surface temperatures (SSTs) alone), PNA increasing in variance with stronger positive and negative phases, and the NP index becoming more strongly negative. These findings imply additional possible increases, to some extent implicit in the model used to generate sea level extremes that is described in Section 5, in the frequency and magnitude of winter storms due to the predominance of El Niño-like conditions (Cayan et al. 1997); in extreme non-tide residual (NTR) water levels (Bromirski et al. 2003) that have been shown to display correlations with positive ENSO phases and the negative NP phase (see Figure 6a); and in both long-period and intermediate-period wave energy, which have demonstrated correlations with PNA and Southern Oscillation Index (similar to ENSO 3.4; Bromirski et al. 2005).

5.0 Projected Sea Level Extremes in California

Although SLR due to climate change is itself a serious concern for California, further concern is raised by the potential impacts that could result from higher baseline sea levels interacting with tides, winter storms, and other episodic events. Extreme high water levels will occur with increasing frequency (i.e., with shorter return period) as a result of mean sea level rise. Many California coastal areas are at significant risk from sea level rise, especially in combination with winter storms (Flick 1998). For example, the city of Santa Cruz is built on the hundred-year floodplain, lying only 20 ft (6 m) above sea level (Hinchliffe and Jones 2002). Levees have been built to contain the 100-year flood; however, as discussed below, a 30 cm (12 in) increase in SLR would shift the 100-year storm surge-induced flood event to once every 10 years. Flooding can create significant damage with enormous financial losses. For example, during the 1997–1998 El Niño winter, abnormally high seas and storm surge caused hundreds of millions of dollars in storm and flood damage in the San Francisco Bay area. Highways were flooded as six-foot waves splashed over waterfront bulkheads, and valuable coastal real estate was destroyed (Ryan 2000).

The frequency of high sea level extremes may be further increased if storms become more frequent or severe as a result of climate change. The increasing duration of high storm-forced sea levels increases the likelihood that they will occur during high tides. The combination of severe winter storms with SLR and high tides that would result in extreme sea levels could expose the coast to severe flooding and erosion, damage to coastal structures and real estate, and salinity intrusion into delta areas and coastal aquifers.

Due to the high coastal impact associated with extreme sea levels, a model was constructed to project future sea level and extremes at California coastal stations. The model is based on the following components:

- Synoptic meteorologically forced sea level fluctuations due to barometric effects (sea level pressure, SLP) and wind stress fluctuations were modeled using a linear regression scheme. This weather variability, extracted from the atmosphere-ocean general circulation model (GCM) simulations, includes local SLP at a tide gauge and regional wind stress. The linear statistical model is based upon on regression of observed sea level non-tidal residuals from tide gages versus local SLP and offshore wind stress from the NCAR/National Centers for Environmental Prediction (NCEP) Reanalysis output, 1950–2004.
- ENSO–related monthly-to-interannual time-scale fluctuations, discussed above, contribute the dominant portion of non-anthropogenic, sea level variability at seasonal-interannual time scales. The ENSO component is also amenable to a simple linear model. Assuming that the same mechanisms will operate in the future as during the historical period, the linear relationship between observed monthly Nino 3.4 SST anomalies and the California station's sea level is used as the ENSO component of the model. ENSO variability was extracted from the 2000–2100 climate model projections using the difference between NINO 3.4 SST and its linear trend over 2000–2100 as a conservative estimate of the ENSO index.

- Astronomical tides are predicted over twenty-first century with good precision based on known tidal constituents (Zetler and Flick 1985a; Munk and Cartright 1966).
- Mean sea level rise was explored from a range of GCM and other model prescribed sea level rise scenarios summarized in Table 3 and Figure 3, as described above. Linear approximations to these sea level rise estimates are superimposed on the astronomical predicted tides, Nino 3.4 SST-related short period variability, and synoptic scale weather components.

Table 3. Projected global sea level rise (SLR) (cm) for the SRES A1fi, A2, and B1 greenhouse gas emission scenarios. SLR for A2 and B1 scenarios is estimated by combining output recent global climate model simulations with MAGICC projections for the ice melt component. SLR estimates for A1fi estimated from MAGICC based upon A2 temperature changes scaled according to those for A1fi.

	B1			A2			A1fi		
	lo	med	hi	lo	med	hi	lo	med	hi
1971-2000	-0.5	-0.2	0.4	-0.5	-0.2	0.3	-0.5	-0.1	0.4
2035-2064	6.0	14.9	31.1	6.3	15.1	28.8	7.1	16.9	32.2
2070-2099	10.9	26.4	53.9	14.2	32.8	60.5	16.8	38.7	71.6

With these components, mean sea level rise values that were estimated for each of two global climate models as driven by two emission scenarios were explored by superimposing the sea level rise onto predicted tides and sea level anomalies produced by model projected weather and El Niño fluctuations. Estimates of potential sea level rise, as discussed above, cover a range from approximately 10 cm (4 in) to about 90 cm (35 in) per hundred years. Reflecting this range, a variety of sea level rise values are considered, with the knowledge that the envelope of potential rates is lowest for the B1 GHG emissions scenario, intermediate for the A2 scenario, and highest for the A1fi scenario. The weather effects on sea level anomalies are derived from model simulated sea level pressure anomalies and wind stress, but the greatest influence is the sea level pressure anomalies. SLP simulated by the models has mean (Figure 8) and variance with good resemblance to that of NCEP reanalysis observations. The effects of ENSO are represented by area average SST anomalies in the Nino 3.4 region (120°W–170°W, 5°S–5°N) extracted from the GCMs and scaled to match the standard deviation of the observed Nino 3.4 series for 1961–1990.

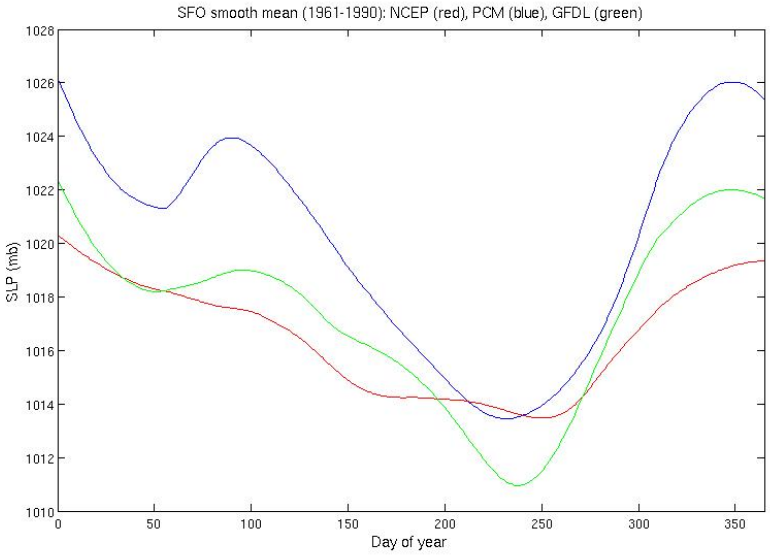

Figure 8. Climatological mean (1961–1990) sea level pressure at San Francisco from NCEP reanalysis in comparison to that from GFDL and PCM historical simulations. Smoothing with a 31-day running mean.

The structure and performance of the linear models, developed from the observed sea level data from Crescent City, San Francisco, and La Jolla is given in Table 4. This shows that the model replicates approximately 50% of the historical daily mean sea level height anomaly variability using three relatively simple weather inputs: SLP, zonal, and meridional wind stress components. The dominant portion of the explained variance by the weather inputs was contributed by anomalous SLP; only about 10% was explained by the wind stress components. The model also included monthly Nino3.4 SST, a commonly used measure of El Niño/Southern Oscillation (ENSO activity, which is known to influence sea level anomalies along the California coast (Chelton and Davis, 1982; Bromirski et al. 2003). The NP and PNA indices did not account for a significant fraction of variance of the sea level anomaly at the three coastal stations, so they were not included as predictors. A reasonable fraction of the monthly to interannual variability of sea level anomaly was explained by Nino 3.4, with approximately 5 cm (2 in) of sea level per ºC of Nino 3.4 SST anomaly, meaning that a significant El Niño having +2ºC SST anomaly will raise sea level height at the coastal stations by about 10 cm (4 in).

The model, developed from the historical dataset, was then applied to "predict" sea level anomalies using climate model weather and Nino 3.4 anomalies, and combined with predicted astronomical sea levels and a prescribed long period trend in mean sea level. For these sea level projections, the model was applied at hourly intervals in order to capture synoptic variability, but this involved a synthetic approach because the climate model data was only available at daily, not hourly, intervals. Sea level pressure was determined to be the most important weather predictor. To construct hourly SLP, a randomly selected daylong sequence of observed hourly SLP from airport weather stations was used to patch in hourly fluctuations about the daily mean. This process

required that: (a) the mean daily SLP from the weather station was within 5 mb of the GCM daily mean, and (b) the first hour of a given day's SLP matched the last hour of the preceding day's SLP within 3 mb in order to retain a relatively realistic and smoothly varying SLP predictor. Hourly wind stress was generated using simple linear interpolation between the daily mean values from the GCM, centered at mid-day.

The fraction of variance explained of the non-tidal sea level anomalies, not including the variability introduced by the long period trend, ranged from 68% at Crescent City to 45% at La Jolla, as shown in Table 4. An example of the simulated sea level anomalies and resultant total sea level height is shown in Figure 9 for the San Francisco station during a two-month period of winter 2006. The variance of the simulated sea level anomaly series followed very closely to that obtained from the observed sea level anomaly. There is also good correspondence between the monthly average of simulated sea level and that from historical observations, as shown in Figure 10 for 2000–2100 Geophysical Fluid Dynamics Laboratory (GFDL)-simulated series in comparison to observed sea level from the San Francisco record. The analogous models, constructed from the A2 and B1 simulations from the PCM GCM, produced quantitatively similar results as those from the GFDL GCM, so they are not shown here.

Table 4. Linear model of non-tide sea level residuals based on reanalysis and Nino 3.4 input as predictors of hourly sea level, 1950–2002. (*a)* Model coefficients and correlation with non-tide residuals, 1950–2002, where non-tide residuals are derived using a 6-month, low-pass filter. (*b)* Correlation between seasonal (Nov–Mar) non-tide residuals and ENSO index from NINO 3.4 SSTs.

(a)	SLP	Tx	Ty	Nino 3.4	R	σ obs	Σ model
Crescent City	1.61	-0.02	0.04	3.61	0.82	17.2	14.2
San Francisco	1.37	0.01	0.04	5.33	0.79	12.3	9.7
La Jolla	1.15	-0.03	0.02	5.49	0.67	8.6	5.7

(b)	R	R^2
Crescent City	0.66	0.44
San Francisco	0.75	0.57
La Jolla	0.85	0.72

As described above, the mean sea level rise values projected by the models ranged from about 10 cm to 90 cm (4 to 35 in) over the 2000–2100 period; this envelope includes the estimated historical rate of sea level rise of approximately 20 cm (8 in) per century observed at the San Francisco and La Jolla tide gages during the last 100 years. Since the rate of historical sea level rise at La Jolla and San Francisco has been close to 20 cm (8 in) per century, the lower end of the model estimated range seems somewhat unlikely.

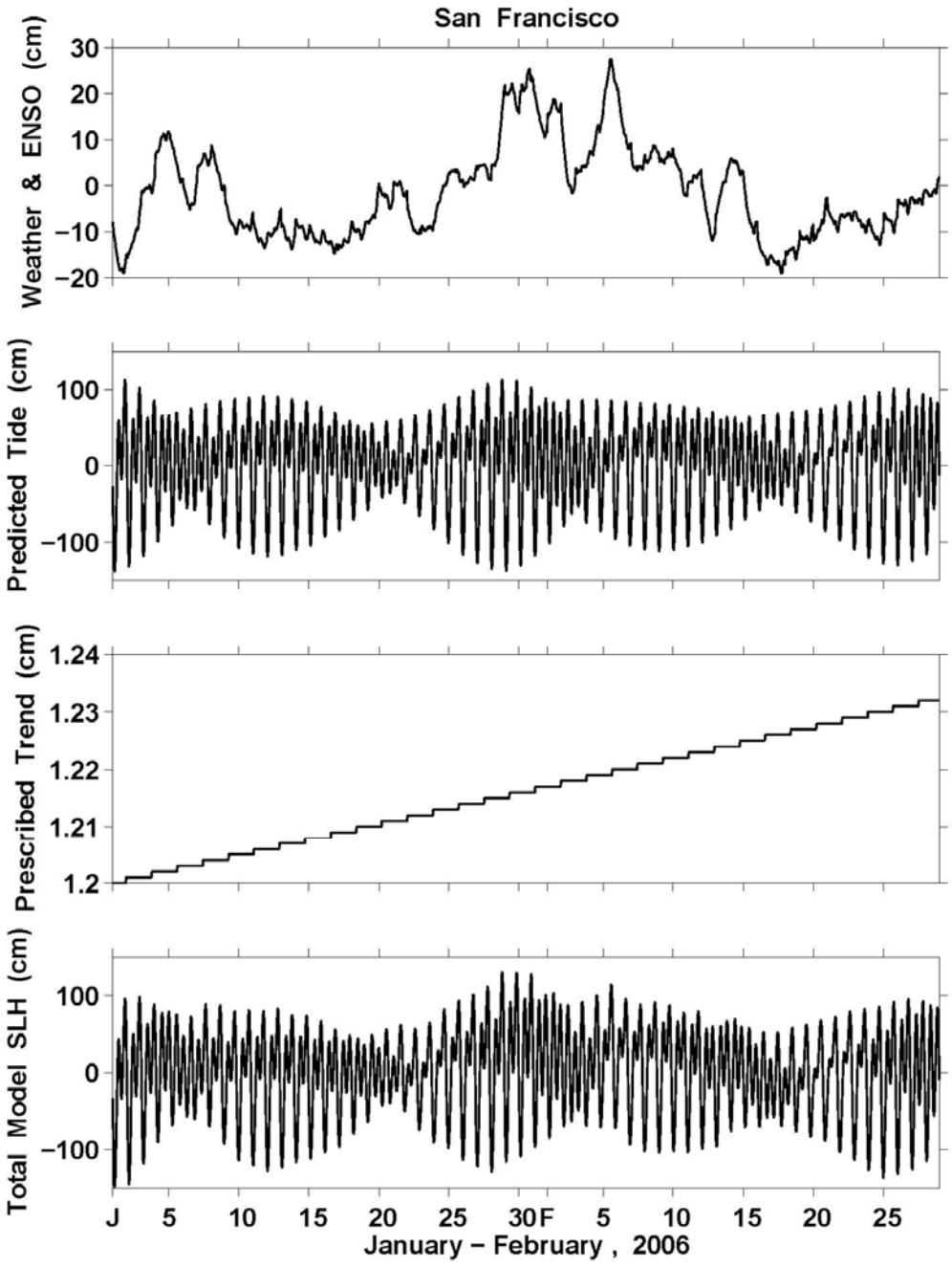

Figure 9. Modeled sea level, including non-tide, astronomical tide-prediction, linear trend (20 cm/year), and total sea level, January–February 2006.

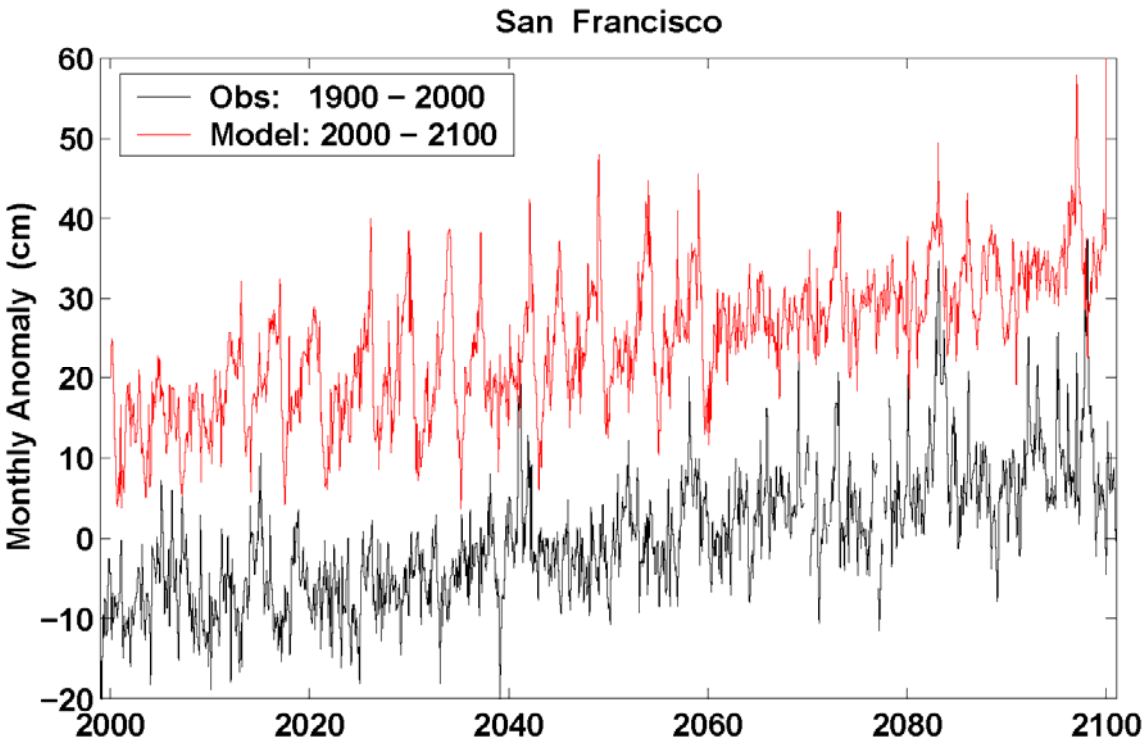

Figure 10. Projected (red) monthly San Francisco sea level anomalies from mean sea level, for 2000–2100 from GFDL A2 model input with linear trend amounting to 20 cm increase, 2000–2100. Observed (black) monthly sea level from San Francisco tide gage (1900–2100) is shown for comparison.

The model results demonstrate how the incidence of sea level extremes is enhanced as sea level rises. The occurrence of extreme events follows a sharply escalating pattern as the magnitude of sea level rise increases. From Table 5, the numbers of sea level events during the 2070–2099 period exceeding the historical 99.99 percentile for the San Francisco tide gage increase from about 25 events/30 years to about 150, to about 1400, to about 7000, to about 20,000 events/30 years as the 2000–2100 sea level change increases from zero to 20 cm, 40 cm, 60 cm, and 80 cm (8 in, 16 in, 23 in, and 31 in), respectively, under meteorological forcing from the GFDL (and PCM) simulations. Figure 11 illustrates the marked increase of sea level extremes as sea level increases (a) over the twenty-first century, and (b) as the upward rise in sea level is increased from zero to 90 cm (35 in) over the 100-year period. The number of extremes varies somewhat between the two models and their respective simulations, but the overall result is identical across each of the model runs, as can be seen by comparing results of the PCM A2 scenario run in Table 6 with the GFDL A2 run in Table 5. A very similar progression of exceedances, in correspondence with a set of increasing sea level trends, occurs from the modeled sea levels at Crescent City (Table 7) and La Jolla (Table 8).

Table 5. Modeled San Francisco sea level exceedances occurring with prescribed MSL trend. 99.9% and 99.99% thresholds, 122.8 cm and 141.0 cm, respectively, are those from observed hourly data at San Francisco 1960–1978. Trends are linear from 2000 to 2100 weather and ENSO impact in sea level simulations from: (*a)* GFDL CM2.1 A2 emissions scenario run, and (*b)* GFDL CM2.1 B1 emissions scenario run.

(a) GFDL A2	2005–2034		2035–2064		2070–2099	
Trend cm/100 yr	99.9%	99.99%	99.9%	99.99%	99.9%	99.99%
0	259	15	286	27	175	23
10	337	19	509	61	575	57
20	445	24	897	112	1611	156
30	619	39	1578	205	3766	529
40	828	63	2634	380	7468	1470
50	1060	97	4113	679	13247	3553
60	1363	139	6114	1238	21170	7072
70	1720	209	8856	2152	31152	12674
80	2146	306	12203	3455	43038	20232
90	2646	433	16334	5235	56613	30048

(b) GFDL B1	2005–2034		2035–2064		2070–2099	
Trend cm/100 yr	99.9%	99.99%	99.9%	99.99%	99.9%	99.99%
0	321	33	250	23	186	15
10	385	47	491	49	582	50
20	488	62	917	89	1611	169
30	629	88	1569	179	3679	536
40	783	110	2699	360	7231	1474
50	1008	146	4292	698	12958	3423
60	1301	186	6430	1241	20836	6791
70	1647	239	9246	2167	30747	12274
80	2062	311	12770	3512	42457	19966
90	2601	405	16981	5419	56026	29595

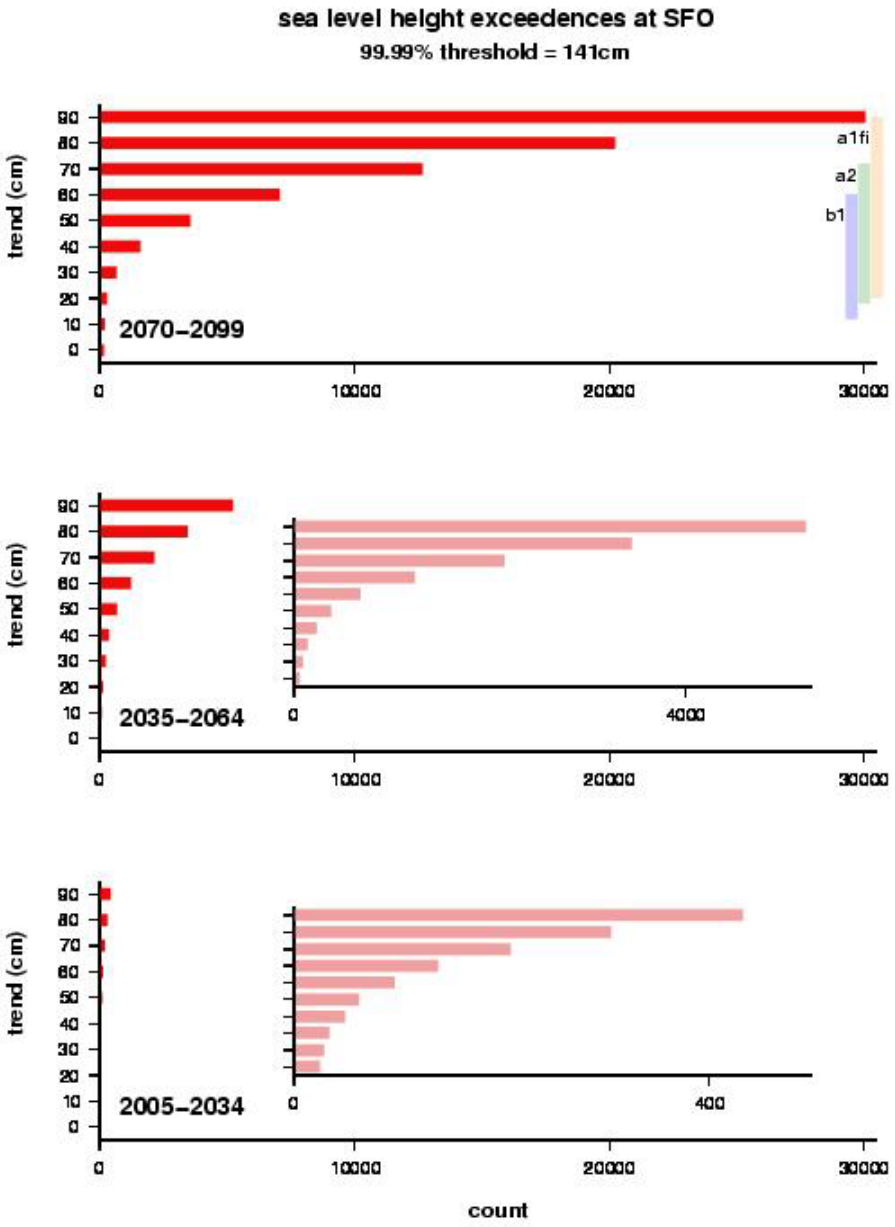

Figure 11. Projected number of hours having exceedances of San Francisco hourly sea level height (SLH) above historical 99.99 percentile from GFDL model weather and ENSO variability superimposed on predicted tides and a range of linear trends, from 0 to 90 cm over 2000–2100. Exceedances are aggregated over 30 years for early, middle, and later periods (2005–2034, 2035–2064, 2070–2099), as shown by the three plots. Inset plots are provided to show lower numbers of exceedances for early and middle periods for lower MSL trends. Range of trends that have been estimated from climate models is indicated for three different GHG emission scenarios is delineated on later period plot.

Table 6. Modeled San Francisco sea level exceedances occurring with prescribed MSL trend. 99.9% and 99.99% thresholds, 141.0 cm and 122.8 cm respectively, are those from observed hourly data at San Francisco 1960–1978. Trends are linear from 2000 to 2100 weather and ENSO impact in sea level simulations from PCM A2 emissions scenario run.

PCM A2	2005–2034		2035–2064		2070–2099	
Trend cm/100 yr	99.9%	99.99%	99.9%	99.99%	99.9%	99.99%
0	225	12	204	10	246	20
10	296	18	431	26	702	69
20	398	28	889	69	1846	209
30	555	44	1614	150	4216	626
40	733	58	2727	326	8222	1698
50	940	88	4277	669	14233	3901
60	1205	121	6495	1286	22647	7721
70	1584	179	9330	2233	32635	13523
80	2028	266	12814	3626	44468	21655
90	2579	384	17104	5550	57944	31435

Table 7. Modeled Crescent City sea level exceedances occurring with prescribed MSL trend. 99.9% and 99.99% thresholds, 174.4 cm and 152.9 cm respectively, are those from observed hourly data at San Francisco 1960–1978. Trends are linear from 2000 to 2100 weather and ENSO impact in sea level simulations from GFDL A2 emissions scenario run.

GFDL A2	2005–2034		2035–2064		2070–2099	
Trend cm/100 yr	99.9%	99.99%	99.9%	99.99%	99.9%	99.99%
0	346	35	294	28	242	34
10	408	42	449	60	505	81
20	479	50	692	103	1034	163
30	563	67	1017	174	1992	335
40	663	87	1520	287	3641	719
50	786	115	2272	447	6382	1480
60	931	148	3210	675	10267	2774
70	1115	186	4464	1002	15775	4966
80	1326	237	6037	1500	22890	8278
90	1572	291	8008	2240	31275	12860

Table 8. Modeled La Jolla sea level exceedances occurring with prescribed MSL trend. 99.9% and 99.99% thresholds, 141.2 cm and 129.0 cm, respectively, are those from observed hourly data at San Francisco 1960–1978. Trends are linear from 2000 to 2100 weather and ENSO impact in sea level simulations from GFDL A2 emissions scenario run

GFDL A2	2005–2034		2035–2064		2070–2099	
Trend cm/100 yr	99.9%	99.99%	99.9%	99.99%	99.9%	99.99%
0	137	5	190	30	125	11
10	208	13	360	59	562	59
20	302	22	691	132	1465	332
30	433	36	1204	292	3065	1028
40	570	75	1962	555	5766	2306
50	756	118	3069	1019	9669	4529
60	984	190	4503	1686	15027	7946
70	1265	296	6407	2700	21765	12667
80	1580	416	8732	4019	30196	18876
90	1972	575	11467	5764	40221	26488

The influence of weather events and ENSO in producing high sea level extremes is evidenced by two additional runs of the statistical model, one with no weather and no ENSO input (Table 9), and one with no weather (Table 10); results of these two runs, along with the one with the entire set of inputs, are illustrated in Figure 12. The first set of simulations ("no weather, no ENSO") indicates that these natural fluctuations are required to produce most of the hourly sea level exceedances above the historical 99.9 percentile threshold and virtually all of those above the 99.99 percentile threshold. As the largest (80–90 cm (31–35 in)/100 year) trends are superimposed and time progresses, these exceedances become more and more prevalent, to the point where at the largest trends during the 2070–2099 period that the exceedances from "no weather, no ENSO" reach about the same level as those for the model with the full set of weather, ENSO, tide, and trend components. The second set of simulations ("no weather') indicate that synoptic scale (a few days) weather disturbances play a critical role in generating extreme sea level extremes, with more than half of the 99.9 and 99.99 percentile level exceedances during the historical period eliminated during the "no weather" run with a low trend imposed. On the other hand, these runs also illustrate the key role played by ENSO in producing sea level extremes, as the exceedances that remain can be attributed to ENSO effects. As with the first set of simulations, if the long period sea level rise is increased, the number of exceedances increases considerably.

Considering the ranges of sea level rise expected for the three emissions scenarios (Figure 4), if warming is modest so sea level rise values are at the low end in each scenario, the increases in extreme events would increase, but not greatly, nor would the three scenarios (B1, A2, A1fi) be differentiated sharply. On the other hand, if warming is large so sea level rise values are at the higher end in each scenario, the incidence of extreme events would increase markedly and the three scenarios (B1, A2, A1fi) could be differentiated sharply. In this case, the highest emission scenario would produce a much greater occurrence of high sea level events.

Acknowledging that there is considerable leeway due to issues such as these arising from the uncertainty in the climate sensitivity, there is still a strong message—in future decades, sea level rise is likely to exceed that which has been observed during the last 100 years or so at tide gages along the California coast, so that historical coastal structure design criteria would more often be exceeded, the duration of events would increase, and these events would become increasingly frequent as sea level rise continues. Because storm-generated waves often coincide with anomalously high sea levels, the impacts of sea level extremes are heightened.

Table 9. Modeled San Francisco sea level exceedances occurring with prescribed MSL trend, no weather, and ENSO included. 99.9% and 99.99% thresholds, 122.8 cm and 141.0 cm, respectively, are those from observed hourly data at San Francisco 1960–1978. Trends are linear from 2000 to 2100 weather and ENSO impact in sea level simulations from GFDL CM2.1 A2 emissions scenario using only predicted tide and imposed trend.

GFDL A2	2005–2034		2035–2064		2070–2099	
Trend cm/100 yr	99.9%	99.99%	99.9%	99.99%	99.9%	99.99%
0	1	0	2	0	1	0
10	12	0	59	0	177	0
20	48	0	303	0	1022	20
30	118	0	819	15	2933	414
40	233	0	1683	130	6433	1581
50	400	1	2965	442	12229	4005
60	637	13	4895	1061	20551	8281
70	921	46	7509	2083	30944	14956
80	1277	119	10931	3540	42953	24060
90	1721	228	15200	5729	56672	34949

Table 10. San Francisco sea level exceedances occurring with prescribed MSL trend, no weather. 99.9% and 99.99% thresholds, 122.8 cm and 141.0 cm, respectively, are those from observed hourly data at San Francisco 1960–1978. Trends are linear from 2000 to 2100 weather and ENSO impact in sea level simulations from GFDL CM2.1 A2 emissions scenario run using Nino 3.4 and pred tide and imposed trend, but without weather.

GFDL A2	2005–2034		2035–2064		2070–2099	
Trend cm/100 yr	99.9%	99.99%	99.9%	99.99%	99.9%	99.99%
0	34	0	20	0	25	0
10	66	0	120	0	268	0
20	111	0	365	0	1167	24
30	200	1	844	6	3123	251
40	310	3	1646	78	6713	1064
50	483	13	2954	259	12722	2912
60	695	24	4795	646	21045	6388
70	1000	51	7426	1291	31422	12107
80	1341	87	10739	2366	43653	20066
90	1798	149	14851	3973	57306	30193

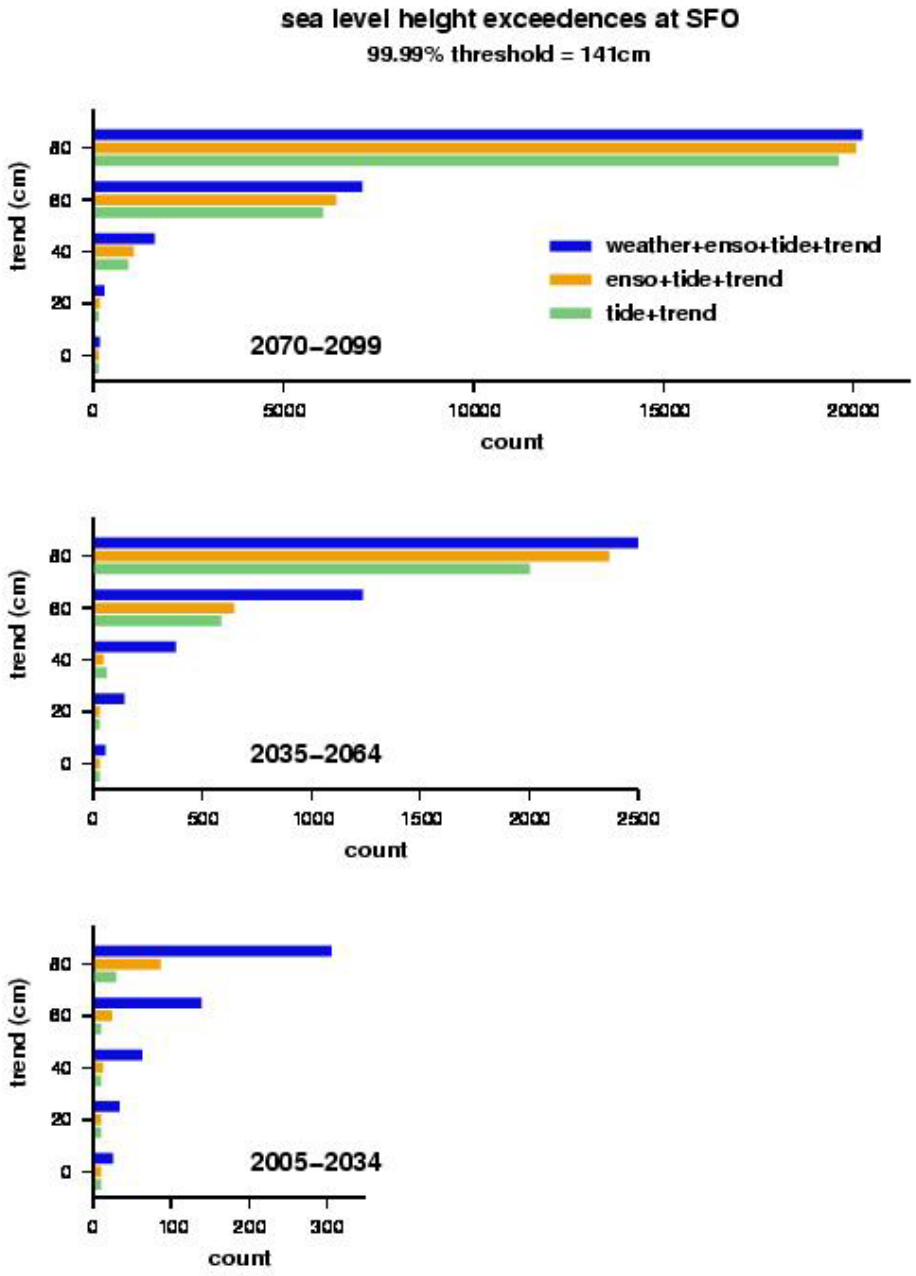

Figure 12. Projected number of hours with exceedances of San Francisco hourly sea level height (SLH) above historical 99.99 percentile from GFDL model, using (a) weather and ENSO variability, (b) only ENSO variability, and (c) no weather, no ENSO variability, superimposed on predicted tides and a range of linear trends, from 0 to 90 cm over 2000–2100. Aggregated exceedances over 30 years for early, middle, and later periods (2005–2034, 2035–2064, 2070–2099) shown by the three plots.

6.0 Possible Impacts to the San Francisco Bay/Delta

In addition to issues associated with inundation and erosion along the open coast of California, sea level rise and attendant flooding may have severe impacts on coastal areas and levee-protected low-lying land such as the San Francisco Bay and Delta. Sea level rise and the resulting elevated storm surges (Bromirski et al. 2003; Bromirski et al. 2005) can also cause saltwater intrusions into estuaries, wetlands, other sensitive surface freshwater systems, and groundwater aquifers. This would damage marginal ecosystems and degrade the quality and reliability of the fresh water supply pumped from the southern edge of the San Francisco Delta (California Environmental Protection Agency 2003).

The risks in the Delta associated with sea level rise are different from simple inundations. Geomorphic processes in the Sacramento-San Joaquin Delta (and Central Valley rivers) of the twenty-first century operate in a landscape dominated by levees and dams. The history of levee breaks in the Delta since 1850 (Figure 13; Florsheim and Dettinger 2005) shows that the numbers of breaks has not declined through time despite engineered changes in upstream river channel structures and morphologies, and despite recent management practices. Major floods have continued to precipitate levee breaches, despite many engineered changes to the rivers and their flows. Projected sea level rises of 20–80 cm (8–31 in) during the twenty-first century can only be expected to compound the vulnerability of subsided Delta Islands to levee failure (described in Mount and Twiss 2005) and increase upstream backwater flooding. In addition to raising water levels generally (in the Delta), sea level rise may be expected to increase the number and duration of extremely high water levels bearing down on the aging Delta levees, mostly by raising the base level upon which the shorter term sea-level fluctuations associated with storms, El Niños, tides, and freshwater flows from river runoff occur. Water level observations from a network of gages from San Francisco inland to Sacramento (Figure 14) indicate that the astronomical tide extends landward through the Delta and into the lower reaches of the Sacramento River, but is damped to less than half of its amplitude at San Francisco by the time it propagates to Sacramento. Notice that this attenuation of tidal fluctuations does not imply that the longest term SLR trends or even many of the slowest tidal, wind, and barometric seal-level signals will be likewise attenuated. Rather, the slowest sea-level fluctuations and changes may be expected to be felt well into the Bay and Delta. However, the short-term tidal fluctuations are attenuated within the Delta and the historical highest water stands have been caused by flood flows from the rivers that enter the Delta from north, east, and south. These flood flows, and the high water levels associated with them, are a prominent feature of water level histories from the Bay and, especially, Delta during fall, winter, and spring (Figure 15).

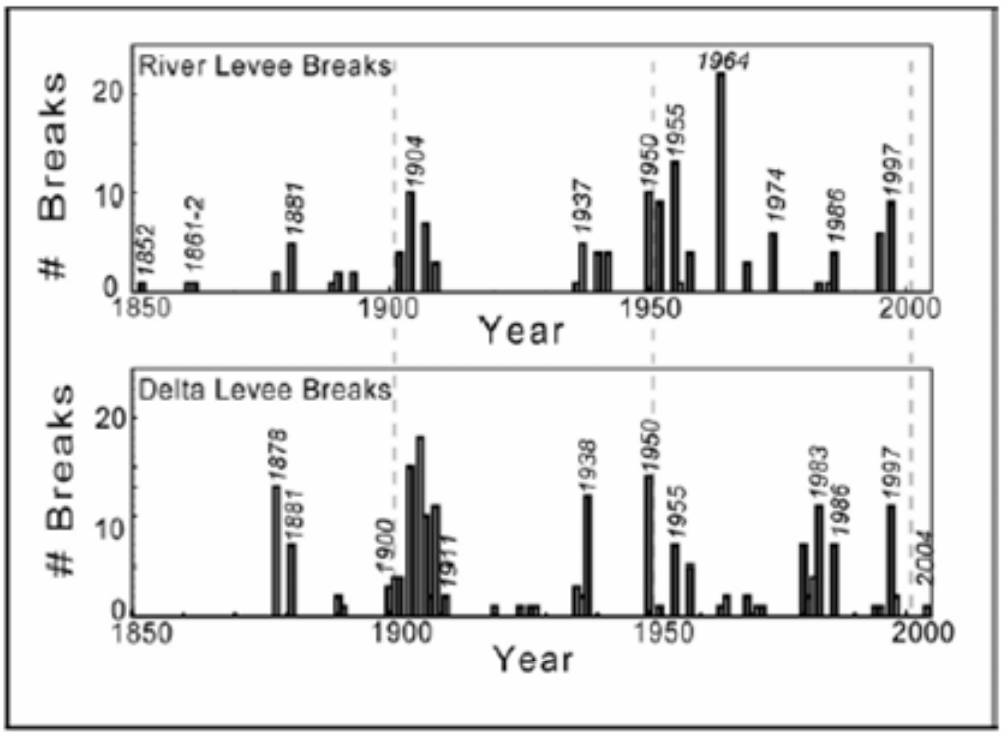

Figure 13. Sacramento and San Joaquin Rivers, tributary, and Delta levee breaks since 1850. Both river and Delta levee breaks are coincident with significant storms that occurred in the late 1800s, the early 1900s, 1937–1938, the mid-1950s, and about every decade since then. Some breaks occur during smaller floods, or for reasons not related to storm hydrology (e.g., the recent Jones Tract Delta levee break in June 2004).

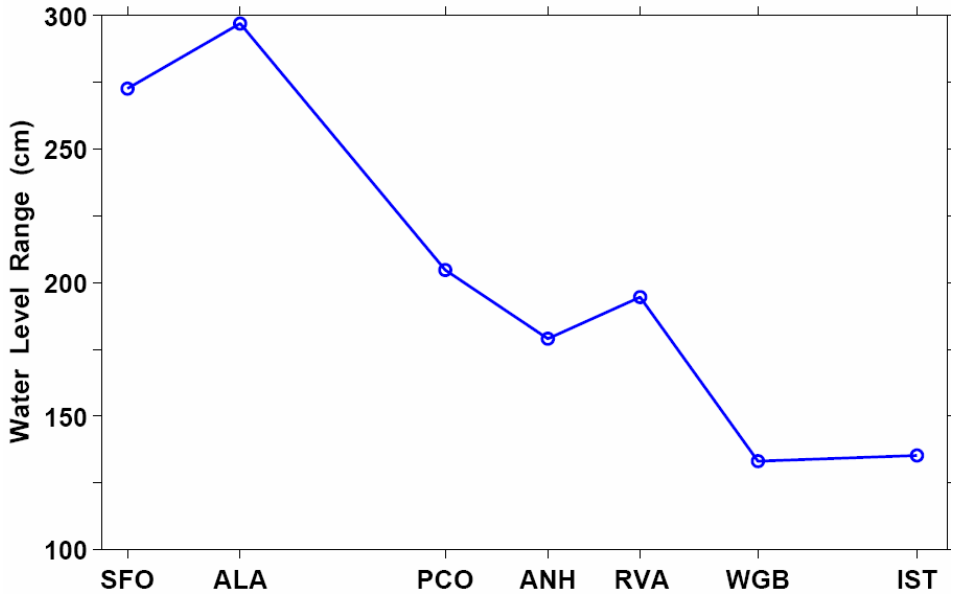

Figure 14. Tide range (cm) at stations from San Francisco near Golden Gate eastward to Sacramento. The ranges were estimated by subtracting the 10 lowest from the 10 highest water level values from all available data during the low river flow May–September periods during 1991 and 1992, except Walnut Grove (WGB), whose record begins in 1993, so the May–September 1993 period was used. Stations include San Francisco at Golden Gate (SFO), Port Chicago (PCO), Alameda (ALA), Antioch (ANH), Rio Vista (RVA), Walnut Grove (WGB), and Sacramento at I Street (IST).

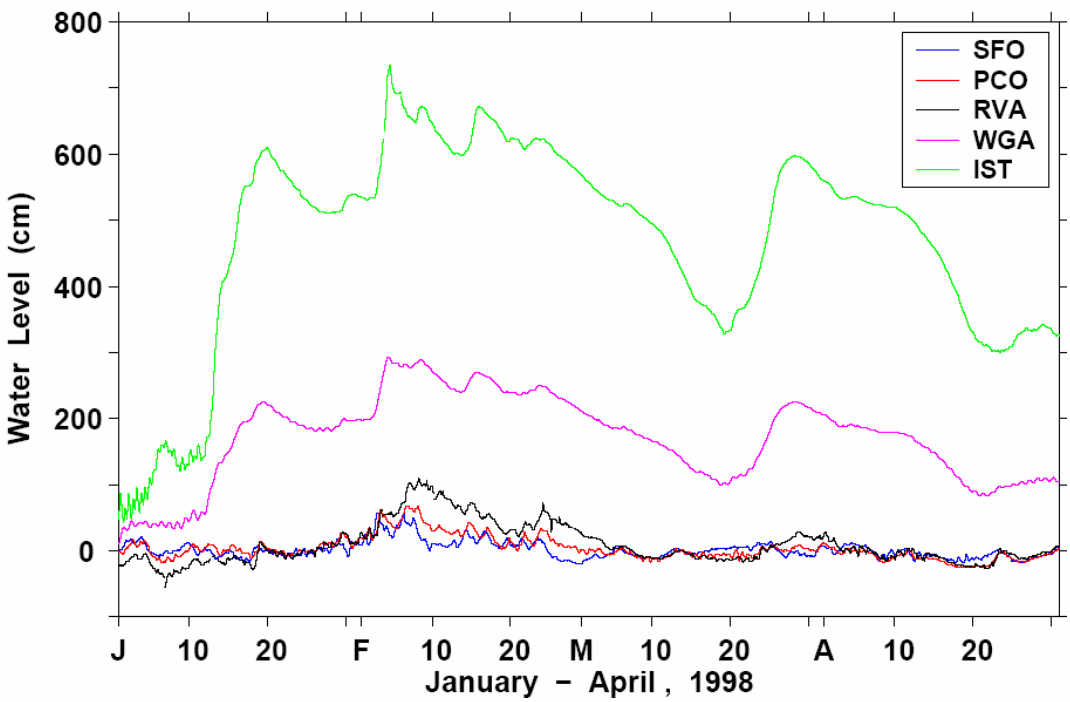

Figure 15. Non-tide water levels (cm) at a series of stations from San Francisco near the Golden Gate eastward to Sacramento for January–April 1998. Stations include San Francisco at Golden Gate (SFO), Port Chicago (PCO), Rio Vista (RVA), Walnut Grove (WGA), and Sacramento at I Street (IST).

In landward locations east of Suisun Bay, the extreme water level elevations rise to several meters above mean low flow levels (Figure 16) in response to freshwater flood flows, compared to historical sea level fluctuations that, by the time they reach the interior of the Delta, may be only about a meter. The mix of flood stages and sea-level changes that develop will determine, to a large extent, important twenty-first century risks to the Delta levees.

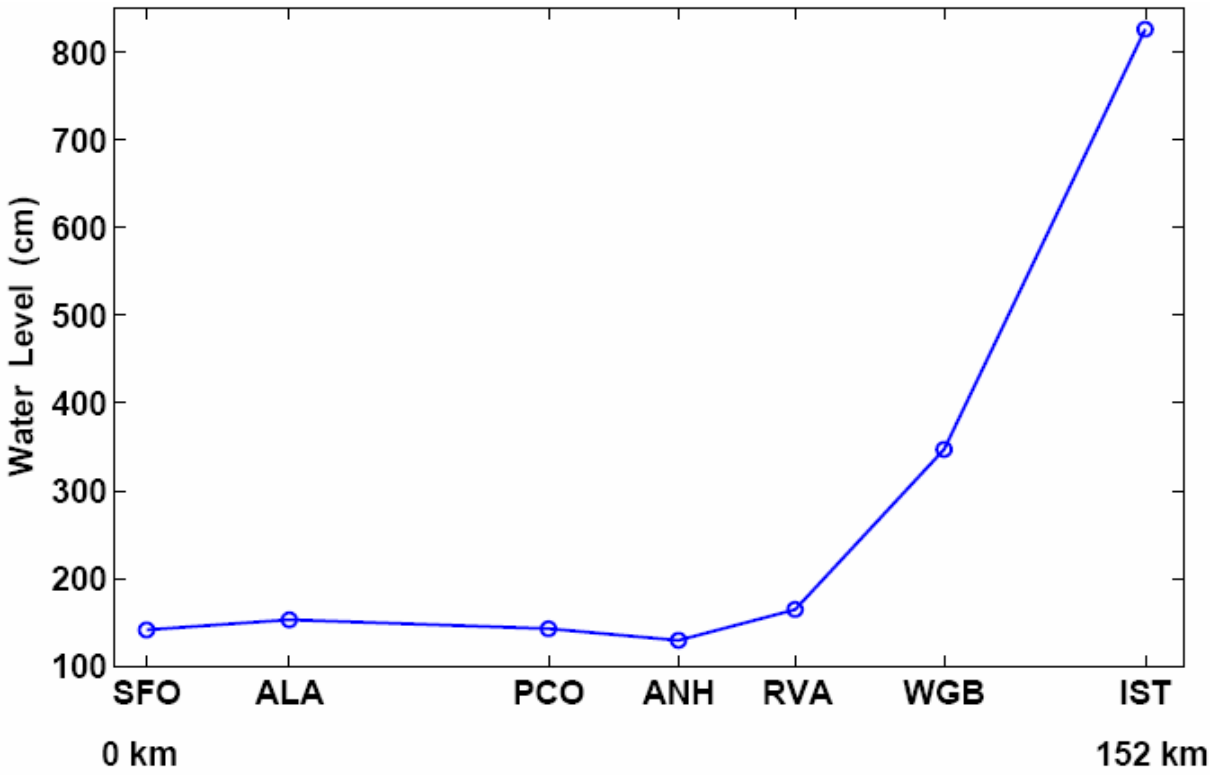

Figure 16. Extreme water elevation (cm) at stations from San Francisco near the Golden Gate eastward to Sacramento. Extreme elevations are the 99.99th percentile levels for 1993–2002, relative to the mean low river flow, from all data within that span (may be different numbers of observations due to different recording gaps). Mean low river flow reference levels were estimated as the mean of the all of the data from the low river flow period during 1991 and 1992. Stations include San Francisco at Golden Gate (SFO), Port Chicago (PCO), Alameda (ALA), Antioch (ANH), Rio Vista (RVA), Walnut Grove (WGB), and Sacramento at I Street (IST).

Along with projected sea-level rise, projected increases in wintertime flows may combine with already-large floods to increase overbank flood extents, erosion, and sedimentation; or alternatively may increase the depth and strength of confined flows and thereby increase the risk of levee failures. If the projected earlier winter runoff is routinely released from reservoirs, in order to maintain flood-control capacity and in the form of relatively constant additions to winter base flows, those additions would increase the duration of bankfull or possibly "levee-full" flows, possibly leading to bank and levee failures through increased saturation and seepage erosion (Florsheim and Dettinger 2005). Mount and Twiss (2005) have argued that the risk of failures of levees in the Delta increases as the *square* of the rise. The idea is simple: the force on the levee increases due to sea level rise in *two* ways: first the higher the sea level the higher the water pressure against the base of the levee, and second, the higher the sea level the larger the levee area experiencing elevated water pressure.

Figure 17a shows—for the San Francisco (SFO) sea-level scenario based on the GFDL climate under A2 emissions and with an assumed sea-level trend of 30 cm (12 in)/century—the counts of hours per year with SFO sea levels above the 99.99% historical sea-level range (in black). Also shown are corresponding counts of how many of those high sea-level stands occurred when SFO sea level pressure was low enough to threaten stormy/wet weather. To estimate this SLP threshold, daily SLPs were regressed against daily flows in the North Fork American River during November-March seasons from 1949–1999 to estimate the general SLP levels associated with various flow levels in central Sierra Nevada Rivers. The 90 historical days with largest flows in the North Fork American River (average of 2/year, top 0.5% of observed flows) were identified, and from those flows, a historical 99.5% exceedance level for flows in the American River was estimated. The SLP threshold corresponding to that flow threshold was then estimated from the flow-SLP regression equation (-4 mb). Using this SLP threshold, the number of hours per year during which sea levels exceeded the 99.99% threshold and, simultaneously, the SLP values were lower than the SLP threshold, were counted (Figure 17, in red).

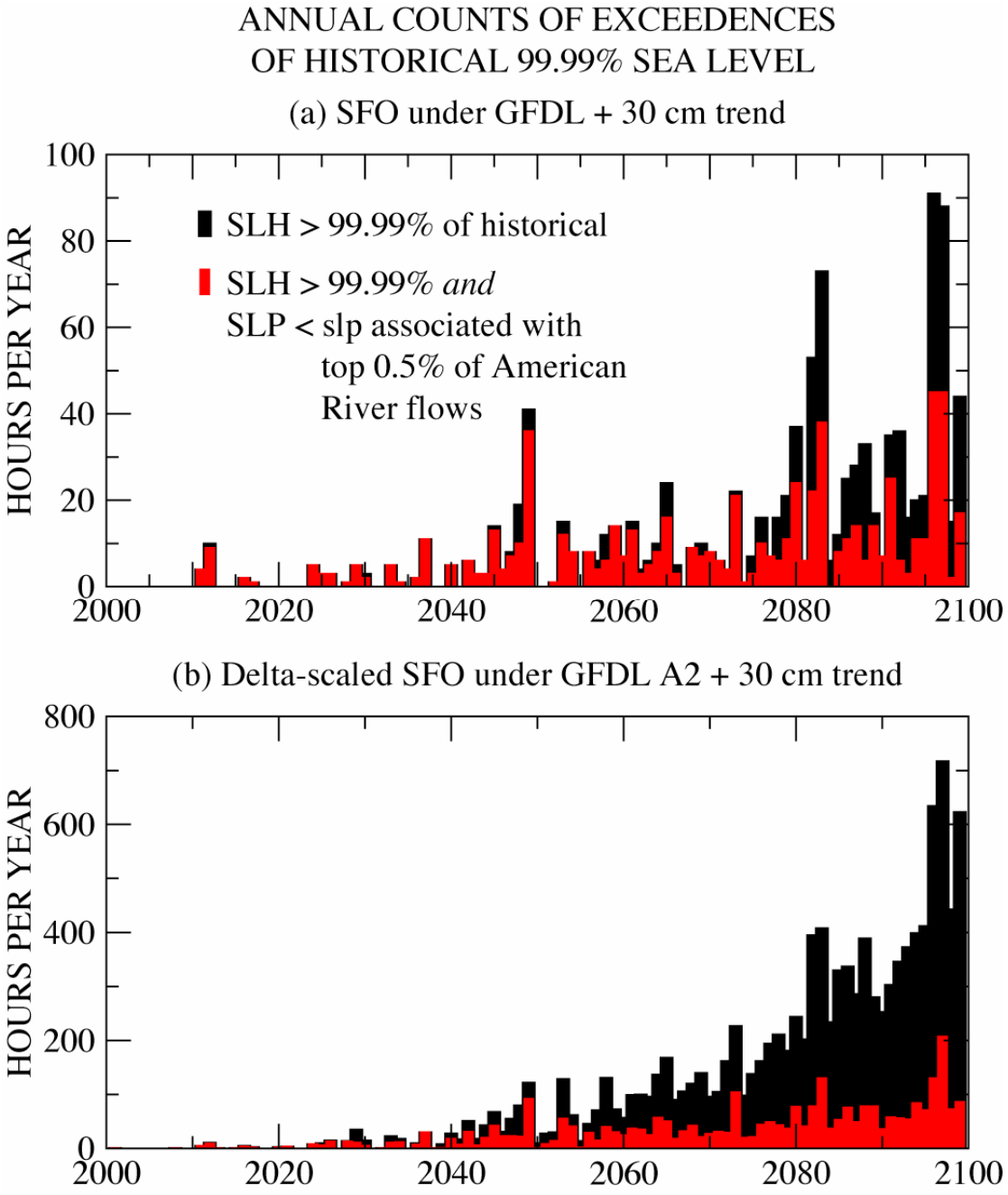

Figure 17. (a) Projected total exceedances of San Francisco hourly sea level height (SLH) above historical 99.99 percentile (black), and number that are coincident with sea level pressure anomalies less than -7 mb, and (b) same as panel (a) except that the nontrending components (and historical 99.99% threshold) of the San Francisco SLH series have been reduced by half to represent attenuation of high-frequency sea-level fluctuations within the Delta. Projected sea level from GFDL model weather and Nino 3.4 SST with a linear trend of 30 cm over 2000–2100.

The count sequence shown indicates that the number of potential storm/high-seas coincidences increases at least until about mid-century and, indeed, makes up most of the increasing numbers of sea-level threshold exceedances until then. Sometime near mid-century, the number of coincidences saturates (becomes more or less stable but still much more common than in the historical period or early decades of the twenty-first century) and the total number of sea-level exceedances, not associated with low SLPs, continues to grow. Thus the coincidences between high sea levels and low SLPs provide most of the occasions when sea levels would have been "almost exceeding" thresholds if the additional trend associated with ocean warming were not there; small trends are sufficient to convert these episodes into exceedances. Only later, when the sea-level trends have reached higher levels, the other "otherwise not close to exceeding" sea levels begin to exceed the threshold. The former "almost exceeding in absence of the trends" episodes are evidently preferentially those occasions when the SLPs are low and thus when storms and floods are more likely. In the Bay and Bay-ward parts of the Delta, this sequence of new sea-level exceedances may suggest that (in the absence of detailed information about the day to day correspondences between sea levels and snowmelt and warming-induced floods, which are not described by the SLP threshold used here) the number of opportunities for high-sea-level stands and floods to coincide might increase most rapidly in the early-to-middle stages of twenty-first century sea-level rise. Later, when the occasions that would (without the trend) almost, but not quite, exceed the sea-level thresholds have largely been converted to exceedances by the sea-level trends, the number of opportunities for coincidence of high sea levels and low SLPs/floods may not grow as much, although the total number of high sea-level stands will continue to grow. Under scenarios with slower sea-level rise, this point beyond which high sea level and low SLP coincidences start to stabilize again may be sometime beyond the end of the twenty-first century; under scenarios of faster sea-level rise (as in Figure 17a), the point may be in mid twenty-first century or earlier.

Further landward in the Delta where the extremes of sea-level fluctuations are attenuated, the coincidence of high sea-level driven stands of water with stormy, potentially flood-prone periods implies smaller enhancements of the flood risks by high sea levels, as indicated by the change in tide ranges as we progress into the upper estuary displayed in Figure 14. However, because the long-term sea-level trends are expected to be less attenuated, they will enhance the frequency of sea-level-driven high-water stands even more rapidly than at locations nearer the ocean. Figure 17b shows the number of times when a 99.99% tide level might be exceeded (black) at a hypothetical location in the Delta where all sea-level signals faster than the long-term trend are attenuated by half, as well as the number of times when these relatively high sea-level-driven stands are accompanied by the low atmospheric pressures associated with winter and spring storms (red). Because the 99.99% threshold of high (sea-level-driven) water-level fluctuations are attenuated along with all the other "fast" fluctuations, the untenanted sea-level rise trends become a larger part of the sea-level variations and many more exceedences develop, along with many more opportunities for the high sea levels to coincide with stormy weather, than at locations closer to the sea (Figure 17a). However, the flood stages are likely to be much higher and the sea-level-driven extreme thresholds lower in the interior of the Delta so that the enhancement of trends in Figure

17b (relative to 17a) need not imply substantially larger levee-breach risks in the former. Notably the numbers of sea-level-driven high water events coinciding with low-pressure systems saturates even more thoroughly (by mid-century) in the Delta-interior example than at SFO.

Another way to view the coincidences of low SLP/high sea levels is to ask how often low SLPs (of the sort that might presage yield storms and floods) would be accompanied by very high sea levels. This count, shown for SFO in Figure 18, is a partial indication of how many potentially stormy periods would be especially dangerous to levees because of concurrent high-sea levels. Figure 18 looks similar to Figure 14, except that the upward trend in the fraction of "potentially stormy" (low SLP) periods that coincide with high sea levels appears to be even more steadily trending than the counts shown in Figure 17. Note that the 3% of "potentially stormy" hours on the y axis of Figure 18 amounts (on average) to about a two-day window per year when the SLPs are low and sea levels are high enough to exceed the historical 99.99% level. The trend in Figure 18 amounts to an increase in the "especially risky" time for the levees from almost never, early in the twenty-first century (at these severe thresholds), to about a day per year at risk by end of century. A similar calculation for the attenuated sea-level fluctuations of the interior Delta (as in Figure 17b) yields an even more steeply trending increase in the number of stormy periods (not shown) that might also be accompanied by (relatively) high sea-level-driven water levels, due (as in Figure 17b) to the relatively untenanted contributions of trends to future sea-level fluctuations in the Delta and the resulting increases in numbers of opportunities for SLP and SLH coincidences.

Finally, the effects of the dependence of levee effects on the square of sea-level rises can be explored preliminarily by considering two sea-level "degree day" indices, that is, the annual sums of hourly sea levels above a given threshold, and of squared hourly sea levels above a given threshold, during times when the threshold is exceeded. Figure 19 shows annual values of these summed values for the SFO sea-level series with assumed 10 and 30 cm (4 and 10 in)/century sea-level trends (bottom and top panels, respectively). All indices in Figure 19 have been normalized by the average indices (for sums of exceedances and sums of squared exceedances, respectively) from the 2000–2010 period in the 10 cm (4 in)/century scenario. The sum-of-squares index, which crudely represents the growth of influence of the sea-level rises on Delta levees, grows about twice as quickly as the unsquared index, which measures the growth of influences of sea-level rises on systems that respond more linearly to the sea levels. Factoring in the attenuation of sea-level fluctuations in the Delta (as in Figure 17b) yields a relatively similar tendency for the squared index to increase by about two to three times as fast as the linear index (not shown). Thus one might, preliminarily, expect risks associated with sea level rise in the Delta and on other tidewater levees to grow about twice as quickly as risks from "simple" inundation.

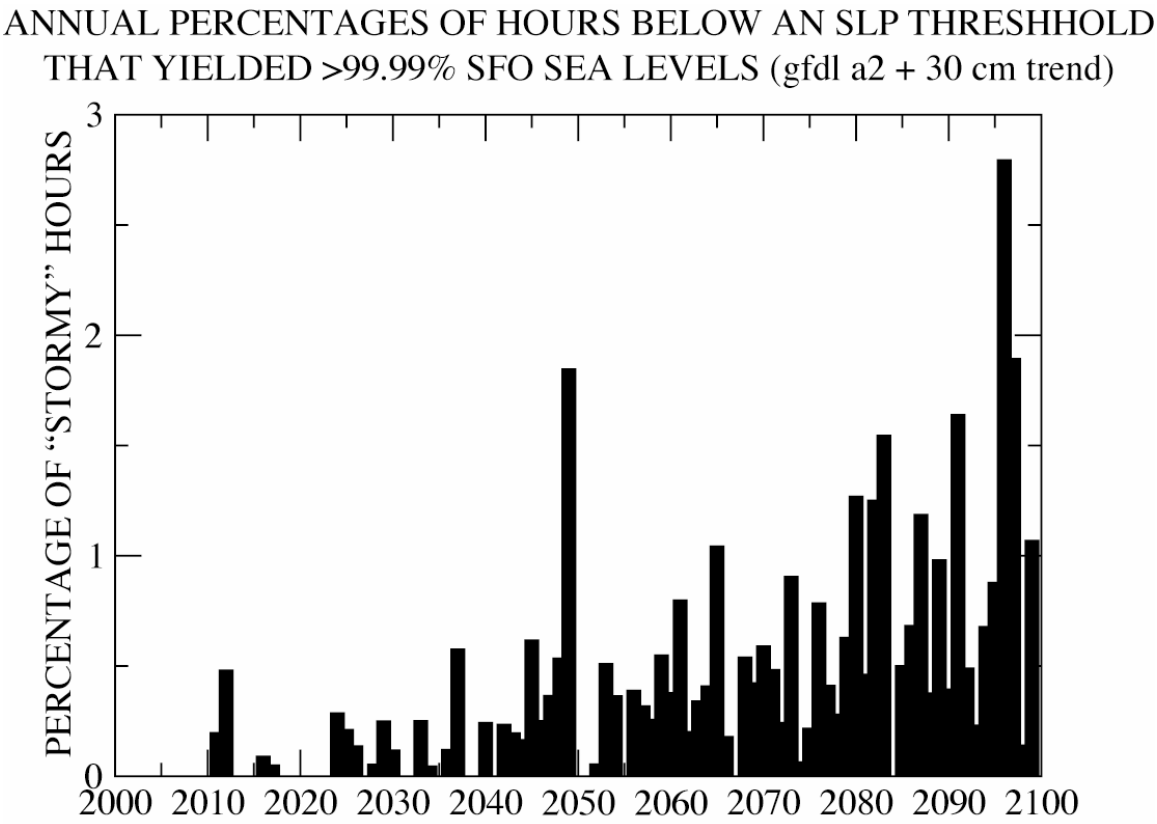

Figure 18. Fraction (%) of hours with SLP below storm pressure threshold that produced sea level above 99.99 percentile, San Francisco. Projected sea level from GFDL model weather and Nino 3.4 SST with a linear trend of 30 cm over 2000–2100.

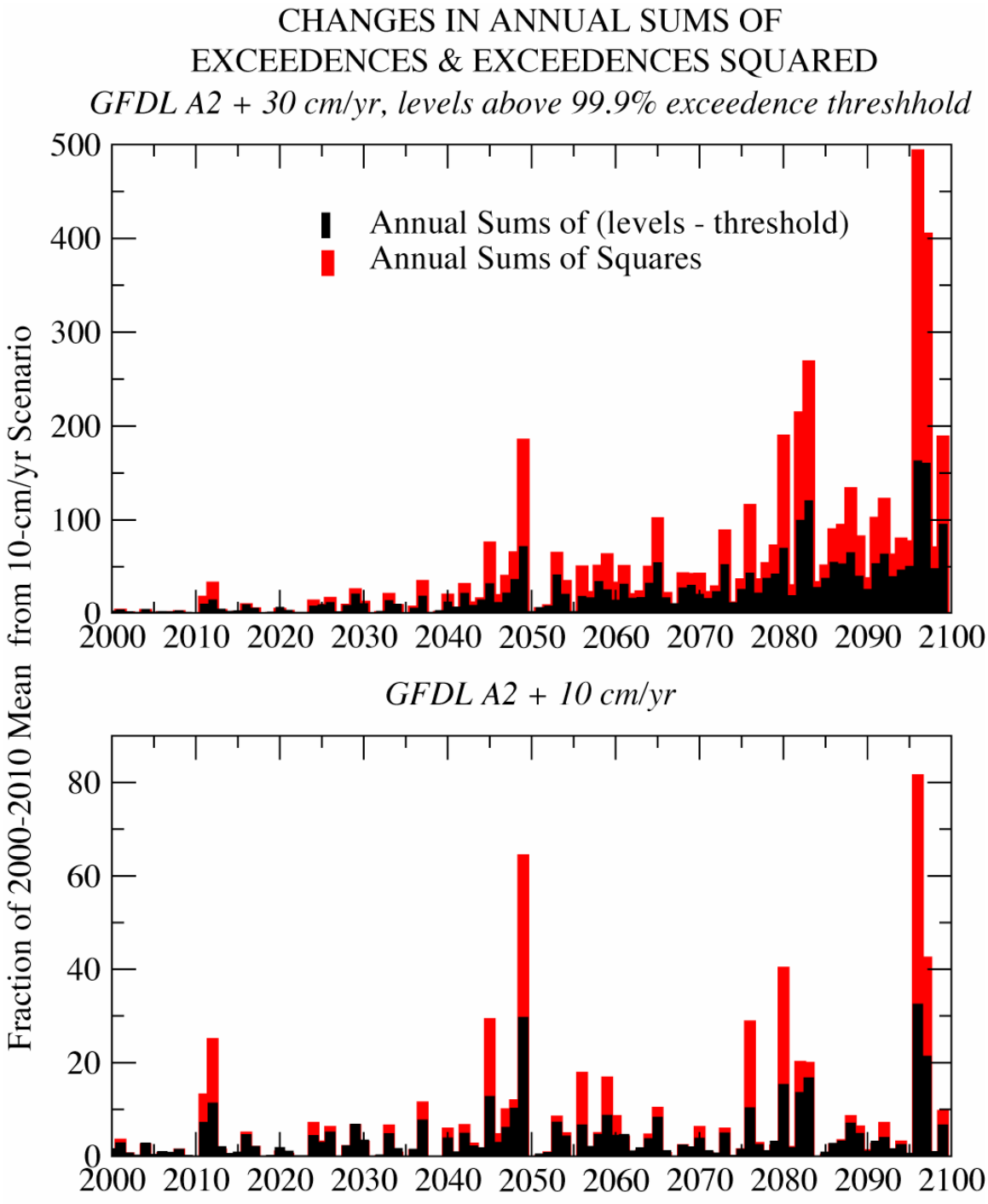

Figure 19. Exceedances and exceedances-squared projected using GFDL model weather and Nino 3.4 with a 30 cm linear trend.

7.0 Waves and Sea Level

Most coastal damage in California occurs during periods when both extreme sea levels and extreme wave heights occur coincidentally (Flick 1998). The additional impact that waves may add to high coastal sea levels can be characterized probabilistically, recognizing that wave amplitudes are related to storminess, which is related to sea level anomalies. The relationship between significant wave height (Hs) and non-tidal sea levels is described using historical wave buoy and sea level records in Northern California (near Crescent City), Central California (near San Francisco), and Southern California (near La Jolla), from approximately 1981–present.

The tendency for higher extreme wave heights and higher extreme non-tide sea level fluctuations increases from the south to the north along the California coast, demonstrated by Gaussian probability distributions of the ranked estimates. These distribution functions would have linear trends if they were purely Gaussian. The most dramatic is the change in wave heights (Figure 20, top) between Pt. Conception (SCA, green) and San Diego (SIO, blue), resulting from shielding of the Southern California Bite coastline by Pt. Conception and the Channel Islands. Differences in the wave energy probability distributions between Pt. Conception and more northern locations near San Francisco (CCA) and Crescent City (NCA) are significant only for extreme events, reflecting consistency of the dominant mode of wave height variability along the central and northern California coasts (Bromirski et al. 2005).

The increased probability of extreme sea level height fluctuations resulting from increasing storm intensity at more northerly coastal locations is evident in the non-tide probability distributions (Figure 20, bottom). The non-tide levels are obtained by spectrally removing the tidal energy from the hourly tide gauge records (Bromirski et al. 2003). Note that the chance of a 30 cm (1 ft) event is much less likely near San Diego (SIO) than near either San Francisco (SFO) or Crescent City (CRE).

Of importance is the probability of the occurrence of extreme waves during extreme sea level height. To illustrate this relationship, this study determined the peak Hs at NOAA buoys near San Francisco during the time periods that the non-tide sea level heights were continuously above the 25th, 50th, 75th, 95th, and 99th percentile thresholds for at least three hours (Figure 21). Because Hs peaks during lower threshold events may also be included in higher threshold events, these functions are not mutually exclusive. The peaks of the resulting conditional probability density functions (PDFs) indicate the most likely peak Hs during the associated non-tide event. The shift of the PDF peak to higher Hs at higher thresholds indicates that higher Hs is more likely during extreme non-tide events than during low amplitude events—this is another aspect of the meteorological forcing which compounds the coastal impacts of high sea levels.

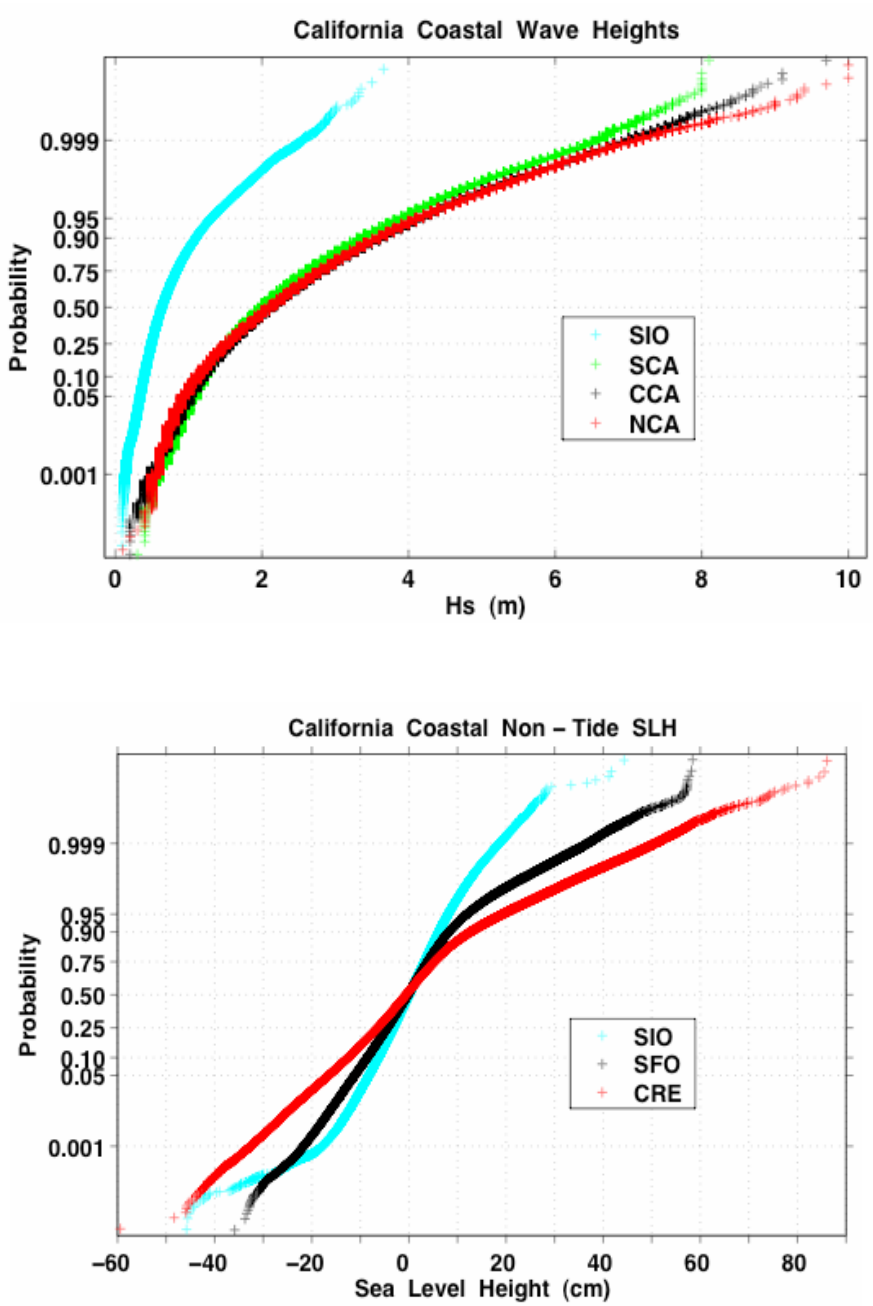

Figure 20. (top) Normal (Gaussian) probability distributions for hourly significant wave height near San Diego (SIO), Pt. Conception (SCA), San Francisco (CCA), and Crescent City (NCA). (bottom) Normal (Gaussian) probability distributions for hourly non-tide sea levels at La Jolla (SIO), San Francisco (SFO), and Crescent City (CRE).

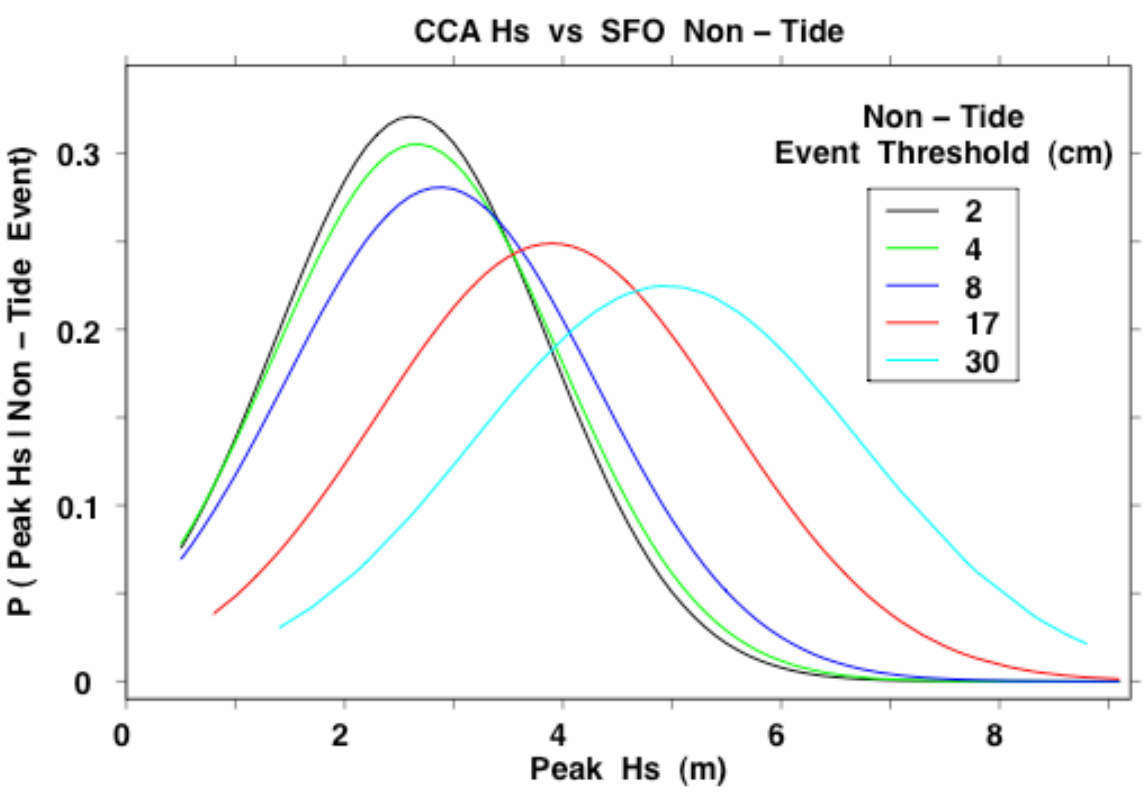

Figure 21. Association of Wave significant wave heights (Hs) at central California coastal buoys with non-tidal sea level anomalies at San Francisco. Each curve represents the conditional probability of Hs during a storm event characterized by non-tidal levels exceeding selected thresholds.

8.0 Summary

Coastal observations and global model projections indicate that California's open coast and estuaries will experience rising sea levels during the next century. Over the last century or so, sea level rise already has affected much of the coast in Southern California, Central California, and the San Francisco Bay and estuary. These historical trends, quantified from a small set of California tide gages, have approached 2 mm/year (0.08 in/year), which are rates very similar to those estimated for global mean sea level. So far, there is little evidence that the rate of rise has accelerated, and indeed the rate of rise at California tide gages has actually flattened since about 1980, but projections suggest that substantial sea level rise, even faster than the historical rates, may occur during the next century.

Recent climate change simulations project significant global sea level rise during the next century due to thermal expansion as the oceans warm and to runoff from accelerated melting of land-based snow and ice. Sea level rise projected from the models increases in proportion to the amount of global warming. By the 2070–2099 period, sea level rise projections range from 13–62 cm (5.1–24.4 in) higher than the 2000 level for simulations following the lower (B1) GHG emissions scenario; from 18–76 cm (7.1–29.9 in) for the medium-high (A2) emission scenario; and from 21–89 cm (8.5–35.2 in) for the higher (A1fi) scenario. It is broadly acknowledged that over the next few centuries, global sea level will likely increase by a meter or more. In the nearer term, these rates of rise will determine how rapidly California will be forced to mitigate and adapt to the problems that elevated sea levels will create.

The sea level rise problem has to contend with several components. Even the largest of the projected sea-level changes over the next century are modest in comparison to the ranges of sea level fluctuations driven, collectively, by tides, weather, and long-term climatic fluctuations. Along the California coast, astronomical tides can cause changes in elevation of about 10 ft (3 m). The most important tidal fluctuations on this coast occur once and twice daily, twice monthly, twice yearly, and every 4.4 years. In addition to relatively steady long-term trends and astronomical tides, sea levels undergo shorter-term fluctuations that carry sea level elevations above and below the predicted tides and longer term changes, in response to weather and to shorter period (months to a few decades) climate fluctuations. The most impressive examples of high sea level episodes in recent decades occurred during the winters of the massive El Niño events of 1982–1983 and 1997–1998 (Flick 1998). Thus, much of the potential damage from rising sea levels will occur during the occasions when high water stands due to tides, weather and climate anomalies are made higher (or more frequent) by the gradually rising mean sea levels. Importantly, GCMs contain El Niños and La Niñas, as well as longer lasting Pacific decadal variability, both in historical simulations as well as in projections that are being used to investigate twenty-first century climate changes.

The present study considers output from two climate models (GFDL and PCM) and three emission scenarios to provide a set of future weather and short period climate fluctuations, and a range of potential long-term sea level rises. Modest to very large sea level rises were projected. The middle to higher end of this range would substantially

exceed the historical rate of sea level rise (15–20 cm (5.9–7.8 in) per century) observed at San Francisco and San Diego during the past 100 years. Using a model of the combined contributions of tides, weather, climate, and long-term global warming on hourly sea levels, the potential for sea level rise impacts was assessed from the occurrence of hourly extremes. Considering a range of climate warming scenarios, and a range of possible sea level trends, we find that if warming is near the low end and associated sea level rise is near the low end, the occurrence of extremely high-sea level events will increase, but not greatly. In this case, the frequency of sea-level extremes under the various emissions scenarios (B1, A2, A1fi) are not much different from each other. On the other hand, if warming is greater, sea level rise trends are at the higher end in each scenario, causing extreme events and their duration to increase markedly, especially for the medium-high and higher GHG emissions scenarios (A2, A1fi). Because of uncertainties in the climate sensitivity, it is not clear how rapidly sea levels will rise, even under the lowest emission scenarios. However, because the modest warming during the past century has already produced rises of sea level that approach 15–20 cm (6–8 in) over the last century, it is prudent to consider scenarios where projected rise rates exceed those modest levels.

Coastal sea level extremes are also exacerbated by other storm effects, such as heavy surf from wind-driven waves. At San Francisco and Crescent City, it is seen that when ocean levels exceed the 99th percentile of the distribution of sea levels from the recent historical record, the average in peak wave height at nearby wave-measuring buoys maintained by NOAA climbs to about double its ambient level. Because wave energy is proportional to the *square* of the wave height, the wave height increase during anomalous sea level episodes is equivalent to a coincident increase in wave energy by a factor of four. Implications are that when anomalous sea level is highest, wave energy has an increased likelihood of reaching very high levels. When these factors coincide with high tides, the chances for coastal damage are greatly heightened. Continuing increases in mean sea level due to global change makes this problem ever more severe.

Sea level rise also threatens the Sacramento/San Joaquin Delta of the San Francisco Bay estuary. Historically, major floods have produced breaches in levees that protect low-lying, subsiding island tracts in the Delta and riverine and estuarine margins elsewhere, despite many engineered changes to the rivers. As sea levels rise, flood stages in the Delta may be expected to rise also, putting more and more pressure on Delta levees. The threats from sea level rise are particularly significant, because as Mount and Twiss (2005) have noted, the forces that rising sea/river levels bring to Delta levees increase as the *square* of the rises, rather than "just" linearly with the rises. Furthermore, the combination of flood and high sea-level stands are particularly dangerous in the Delta, where it is the combination of sea level and river stages that determine the water height. Storms are primary causes of the highest water levels both from barometric and wind effects on the sea levels and from the (freshwater) floods that they can generate. Projections of the number of projected extremely high sea level episodes at San Francisco that coincide with potentially storm/flood episodes suggests that, at least during the earlier decades of the next century, the largest increases in the frequency of extremely high sea level episodes as sea levels rise will coincide with periods of enhanced storm-flood risks.

9.0 References

Andrews, E. D., R. C. Antweiler, P. J. Neiman, and F. M. Ralph, 2004: "Influence of ENSO on Flood Frequency along the California Coast." *J. Climate* **17:** 337–348.

Barnston and Livezey, 1987: "Classification, seasonality and persistence of low-frequency atmospheric circulation patterns." *Mon. Wea. Rev.* **115:** 1083–1126

Barnett, T. P., 1984: "The estimation of "global" seal level change: A problem of uniqueness." *J. Geophys. Res.* **89**(C5): 7980–7988.

Bromirski, P. D., R. E. Flick, and D. R. Cayan, 2003: "Storminess Variability along the California Coast: 1858–2000." *J. Climate* **16:** 982–993.

Bromirski, P. D., R. E. Flick, D. R. Cayan, and N. Graham, 2004: "California Coastal Sea Level and Wind Wave Variations during the Historical Record." California Energy Commission Presentation.

Bromirski, P. D., D. R. Cayan, and R. E. Flick, 2005: "Wave spectral energy variability in the northeast Pacific." *J. Geophys. Res.* **110:** C03005, doi:10.1029/2004JC002398.

Cabanes, C., A. Cazenave, and C. Le Provost, 2001: "Sea Level Rise During Past 40 Years Determined from Satellite and In Situ Observations." *Science* **294:** 840–842.

Cane, M., 2005: The evolution of El Niño, past and future. *Earth & Planetary Sci Letters* 230: 227–240.

Cayan, D., 1996: "Interannual climate variability and snowpack in the western United States." *J. Climate* **9:** 928–948.

Cayan, D. R., K. T. Redmond, and L. G. Riddle, 1999: "ENSO and hydrologic extremes in the Western United States." *J. Climate* 12(9) : 2881–2893.

Chambers, D. P., C. A. Mehlhaff, T. J. Urban, D. Fujii, and R. S. Nerem, 2002: "Low-frequency variations in global mean sea level: 1950–2000." *J. Geophys. Res.* **107**, Art. No. 3026.

Chelton, D. B., and R. E. Davis, 1982: "Monthly mean seal-level variability along the west coast of North America." *J. Phys. Oceanogr.* **12:** 757–784.

Church J. A., J. M. Gregory, P. Huybrechts, M. Kuhn, K. Lambeck, M. T. Nhuan, D. Qin, and P. L. Woodworth, 2001: "Changes in sea level. Chapter 11 of the *Intergovernmental Panel on Climate Change Third Assessment Report*," Cambridge University Press, Cambridge, 639–694.

Church, J. A., N. J. White, R. Coleman, K. Lambeck, and J. X. Mitrovica, 2004: "Estimates of the regional distribution of sea level rise over the 1950–2000 period." *J. Climate* **17:** 2609–2625.

Cobb, K. M., C. D. Charles, H. Cheng, and R. L. Edwards, 2003: "El Niño/Southern Oscillation and tropical Pacific climate during the last millennium." *Nature* **424:** 271–276.

Cubash, U., G. A. Meehl, et al., 2001: *Projections of Future Climate Change.* Chapter 9, IPCC Third Assessment Report of the Intergovernmental Panel on Climate Change. Cambridge University Press, Cambridge, UK, and New York, New York. 2001.

Dettinger, M. D., D. S. Battisti, R. D. Garreaud, G. J. McCabe, and C. M. Bitz, 2001: Interhemispheric effects of interannual and decadal ENSO-like climate variations on the Americas, in V. Markgraf (ed.), *Interhemispheric climate linkages: Present and Past Climates in the Americas and their Societal Effects:* Academic Press, 1–16.

Dettinger, M. D., D. R. Cayan, G. M. McCabe, and J. A. Marengo, 2000: Multiscale streamflow variability associated with El Niño/Southern Oscillation, in H. F. Diaz and V. Markgraf, (eds.), *El Niño and the Southern Oscillation--Multiscale Variability and Global and Regional Impacts:* Cambridge University Press, 113–146.

Diaz, H. F., M. P. Hoerling, and J. K Eischeid, 2001: "ENSO variability, teleconnections and climate change." *Intl J. Climatology* **21**(15): 1845–1862.

Douglas, B. C, and W. R. Peltier, 2002: "The puzzle of global sea level rise." *Physics Today* 35–40, 2002.

Ely, L. L., 1997: "Response of extreme floods in the southwestern United States to climatic variations in the late Holocene." *Geomorphology* **19**: 175–201.

Enfield, D. B., and J. S. Allen, 1980: "On the structure and dynamics of monthly mean sea level anomalies along the Pacific coast of North and South America." *J. Phys. Oceanogr*. **10**: 557–578.

Fairbanks, R. G., 1989: "A 17,000-year Glacio-eustatic Sea Level Record: Influence of Glacial Melting Rates on the Younger Dryas Event and Deep-Ocean Circulation." *Nature* **342**: no. 6250, 637–642.

Flick, R. E., and D. R. Cayan, 1984: Extreme Sea Levels on the Coast of California, ASCE, 19th Coastal Engineering Conference Proceedings, Houston, Texas, pp. 886–897.

Flick, R. E., 1986: "A review of conditions associated with high sea levels in Southern California." *Sci. Tot. Env.* **55**: 251–259.

Flick, R. E., 1998: "Comparison of California tides, storm surges, and mean sea level during the El Niño winters of 1982–1983 and 1997–1998." *Shore and Beach* **66**(3), 7–11.

Flick, R. E., 2000: "Time-of-Day of Peak Tides in a Mixed-Tide Regime." *Shore & Beach* **68**(4): 15–17.

Flick, R. E., and A. Badan-Dangon, 1989: "Coastal Sea Levels During the January 1988 Storm off the Californias." *Shore & Beach* **57**(4): 28–31.

Flick, R. E., and D. R. Cayan, 1984: "Extreme Sea Levels on the Coast of California," *Proc. 19th Int. Conf. Coastal Eng*., Amer. Soc. Civil Eng., 886–898.

Flick, R. E., J. F. Murray, and L. C. Ewing, 2003: "Trends in United States Tidal Datum Statistics and Tide Range." *J. Waterway, Port, Coastal and Ocean Eng*. Amer. Soc. Civil Eng., **129**(4): 155–164.

Florsheim, J., and M. Dettinger, 2005: "Influence of anthropogenic alterations on geomorphic response to climate variations and change in San Francisco Bay-Delta and watershed. " *Watershed Management Council Networker* 13, Spring 2005, 13–16.

Hanley et al., 2003: "A quantitative evaluation of ENSO indices." *J. Climate* **16**: 1249–1258

Hinchliffe, G., and E. Jones, 2002: Coastal and River Flooding in Santa Cruz, California. Santa Cruz Field Course, University of Liverpool, 75–77.

Hulme, M., S. C. B. Raper, and T. M. L. Wigley, 1995: "An integrated framework to address climate change (ESCAPE) and further developments of the global and regional climate modules (MAGICC)." *Energy Policy* **23**: 347–355.

Mantua, N. J., S. R. Hare, Y. Zhang, J. M. Wallace, and R. C. Francis, 1997: "A Pacific interdecadal climate oscillation with impacts on salmon production," *Bull. Am. Met. Soc*. **78**: 1069–1079.

Masutani, M., and A. Leetmaa, 1999: "Dynamical mechanisms of the 1995 California floods." *J. Climate* **12**: 3220–3236.

Mount, J., and R. Twiss, 2005: "Subsidence, sea level rise, and seismicity in the Sacramento-San Joaquin Delta." *San Francisco Estuary and Watershed Science* 3:1 (March 2005), Article 5.

Moy, C. M., G. O. Seltzer, D. T. Rodbell, and D. M. Anderson, 2002: Variability of El Niño/Southern Oscillation activity at millennial timescales during the Holocene epoch. *Nature* 420: 162–165.

Munk, W. H., 2002: "Twentieth century sea level: An enigma." *Proc. Nat. Acad. Sci*. **99**(10), 6550–6555.

Munk, W. H., and D. E. Cartwright, 1966: "Tidal spectroscopy and prediction. *Phil. Trans. Roy. Soc. London*, **259**: 533–581.

Nakićenović, N., J. Alcamo, G. Davis, B. de Vries, J. Fenhann, S. Gaffin, K. Gregory, A. Grübler, T. Y. Jung, T. Kram, et al., 2000: *IPCC Special Report on Emissions Scenarios.* Cambridge University Press, Cambridge, United Kingdom and New York, New York.

Nerem, R. S., D. P. Chambers, E. W. Leuliette, G. T. Mitchum, and B. S. Giese, 1999: "Variations in global mean sea level associated with the 1997–1998 ENSO event: Implications for measuring long term sea level change." *Geophysical Research Letters* **26**(19): 3005–3008.

NOAA, Pacific Marine Environmental Laboratory, 1998: 1997–98 El Nino Sea Level. Monthly Mean Sea level for U.S. West Coast, Alaska, Hawaii. www.pmel.noaa.gov/tsunami/Sea_level_1997_98/sea_level_1997_98.html.

Rein, B., A. Luckage, R. Lutz, F. Sirocko, A. Wolf, C-W. Dullo, 2005: El Niño variability off Peru during the last 20,000 years. *Paleoceanography,* 20, PA4003 (1–17), doi:10.1029/2004PA001099.

Robertson, A. W., and M. Ghil, 1999: "Large-scale weather regimes and local climate over the western United States." *J. Climate* **12**: 1796–1813.

Ryan, H., H. Gibbons, J. W. Hendley, and P. Stauffer, 2000: El Niño sea-level rise wreaks havoc in California's San Francisco Bay Region. USGS Fact Sheet 175–99. Available online at: http://geopubs.wr.usgs.gov/fact-sheet/fs175-99/ .

Trenberth, K., and J. Hurrell, 1994: "Decadal atmosphere-ocean variations in the Pacific." *Climate Dynamics* **9**: 303–319.

Trenberth, K. E., and T. J. Hoar, 1997: "El Niño and climate change." *Geophysical Research Letters* **24**(23): 3057–3060.

Tudhope, A. W., C. P. Chilcott, M. T. McCulloch, E. R. Cook, J. Chappell, R. M. Ellam, D. W. Lea, J. M. Lough, and G. B. Shimmield, 2001: Variability in the El Niño-Southern oscillation through a glacial-interglacial cycle. *Science* 291: 1511–1517.

Tudhope, S., and M. Collins, 2003: "Global change—The past and future of El Niño." *Nature* **424**(6946): 261–262.

Wells, L. E., 1990: Holocene history of the El Niño phenomenon as recorded in flood sediments of northern coastal Peru. *Geology* **18**: 1134–1137.

Westerling, A., 2001: Climate variability and large storm surge on the Pacific coast of the United States. Presented at the 81st Annual Meeting of the American Meteorological Society, January, 2001.

Zelle, H., G. Van Oldenborgh, G. Burgers, and H. Dijkstra, 2005: El Niño and Greenhouse warming: Results from ensemble simulations with the NCAR CCSM. *J. Climate*, **18**: 4669–4683.

Zetler, D. B., and R. E. Flick. 1985a: "Predicted extreme high tides for mixed tidal regimes." *J. Phys. Oceanogr.* 15(3), 357-359.

Zetler, B. D., and R. E. Flick. 1985b: "Predicted Extreme High Tides for California, 1983–2000." *J. Waterway Port, Coastal and Ocean Eng*. Amer. Soc. Civil Eng., 111(4) : 758-765.